TEP4175
Numerical simulation of the airborne transmission of COVID-19 due to respiratory activities under different ventilation conditions

Spring 2021

MASTER THESIS

Allan Quesnel

0.1 Abstract

Covid-19 pandemic have recently raised lots of issues about the way we lived socially and have led to various studies for our social behaviour to be adapted to struggle the crisis. This report presents the work done during the master thesis regarding this virus contamination. The goal of this thesis was to understand and evaluate the infection risk under different ventilation conditions, between a standing and infected person, and a sitting one. Therefore, a CFD study has been performed in parallel with another thesis containing relevant experiment data. To achieve a model coherent with this data, we use a whole process: literature review to collect data and get used to CFD problems in indoor environment, simplified geometry and mesh to understand the available CFD models, mesh study to perform efficient and accurate calculations, additional experiments to improve the model, After validating the model with experimental data, we can observe the virus concentration in the room and deduce which configuration is the best to limit contamination. CFD study shows the experiments realized hide some critical points where the risk of infection is the highest during the exhalation of the infected person.

Contents

1 Summary

In recent years, numerous review papers have been published dealing with contamination in indoor environment due to the sanitary crisis of the covid-19. These reviews focused on different main subjects and always targeted some particular conditions. Covid-19 infections can occur in three different ways: direct contamination, aerosols remaining in the air and contaminated objects. These 3 ways come from the airborne release mechanism of covid19 in indoor environment [1]. Particles will be expulsed during exhalation period and each particle, regarding its size, will be affected differently by airflow patterns. Figure 1 presented by Borbar and al., depicts two kinds of transmission according to droplet size and flow patterns. Around the mouth, on average the well-known 1-meter security distance, short-range transmission is controlled by the initial advection of exhaled respiratory droplets where fine particles evaporate into droplet nuclei and large particles (¿100um [1]) deposits on near surfaces due to gravity settling. Above this distance, long-range transmission occurs, and droplet nuclei are transported thanks to ventilation air supply systems, turbulent mixing in the room and thermal plume (figure 1).

Jianchao Ma and al. [2] have found that the critical velocity when the thermal plume can be neglected in indoor environment under DV conditions was around 0.30 m/s. For lower velocities, the flow is distracted by the human thermal plume due to the temperature difference between body surface and room. According to Sun and al. [3], this can lead to transportation of aerosols from lower regions to breathing zones. Gravity settling combined with thermal plume can then be a source of contamination, that is why buoyancy effects are considered in every CFD simulation aiming at describing contamination processes. Chudecka and Lubwowska [4] have determined with high accuracy the surface temperature distribution in women dividing body into different parts: chest, back, arms, hands, thighs and shanks.

This data, combined with computational thermal manikin (CTM), can be used for modern CFD studies and more complex indoor problems. Computational Fluids Dynamics in ventilation design book [5] has summed up everything one needs to know about CFD in indoor environment. Typical theory, models and boundary conditions are presented. It also shows how the mesh can be structured with cell number and wall yplus requirements. A lot of CFD simulations have been performed during recent years depicting the dispersion and evolution of airborne particles. Sheikhnejad and al. [6] have in fact sorted main studies from 2005 to 2020 in this field using different particle models as Discrete Phase Model (DPM), Species Transport and Euler-Lagrangian method. The first model associates each particle with a diameter size to study the repartition of particles of same diameter while the second one models viruses as homogeneous gas which may be correct in some cases under specific assumptions.

The choice of such a model can also depend on which breathing mode one wants to develop. Main modes considered are normal breathing, talking, sneezing and coughing. Gao and Niu [6] have studied infection risk due to transient respiration process. Sinusoidal and slot math functions were used for
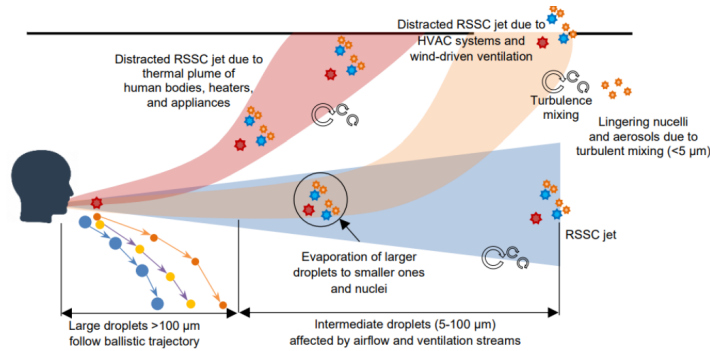
Figure 1: Airborne transmission process

2 List of symbols and abbreviations

The following table groups together all the common symbols and abbreviations we might have used in the report to describe some parameters or methods.

Symbol	Unit	Parameter
CTM		Computational Thermal Manikin
$HVAC$		Heating, ventilation, air conditioning
CFD		Computational fluid dynamics
TP		Thermal plume
ACH	[-]	Air changes per hour
Re	[-]	Reynolds number
ρ	$[kg/m^3]$	Air density
T	$[K]$	Temperature
V	$[m^3]$	Volume
u	$[m/s]$	Velocity
q	$[m^3/s]$	Volumetric flow rate
k	$[m^2/s^2]$	Turbulent kinetic energy
ϵ	$[m^2/s^3]$	Turbulent kinetic dissipation
ω	$[s^{-1}]$	Vorticity
ν	$[m^2/s]$	Kinematic viscosity
I	[-]	Turbulence intensity
D_h	$[m]$	Hydraulic diameter
g	$[m/s^2]$	Gravity
τ	[]	Friction shear stress
y_p^+	[-]	Dimensionless distance to wall
N	[-]	Number of cells
h	$[m]$	Height of supply slot
f	$[N/m]$	Force per unit volume
β	$[K^{-}1]$	Volumetric thermal expansion coefficient
μ_t	$[kg/(m.s)]$	Turbulent viscosity
L	$[m]$	Length of the room
W	$[m]$	Width of the room
H	$[m]$	Height of the room
M_{inf}		Infected (standing) manikin
M_{exp}		Exposed (sitting) manikin

3 Introduction

3.1 Introduction

COVID-19 has affected people worldwide during the sanitary crisis from 2019 to nowadays and a lots of scientific studies have been developed so that we may understand better how it behaves and transmit from one human to another. In this thesis, We will focus on creating a Numerical model to estimate the concentration of contaminant in a laboratory room, previously used for experiments. This room depicts a typical office size with a board, tables and HVAC systems. Then it is mandatory to examine the ins and ours of indoor environment problems to model correctly both ventilation systems and room geometry. Moreover, we have to combine these with some of the main fluid mechanics features which will intervene in this thesis such as turbulence, playing a major role in mixing and diffusion of airflow.

Depending on such models, adapted meshing and set up allow depicting, with good accuracy, real phenomena. To make these numerical models suited with real situation, we need to explore theoretical requirements, suggestions, definitions , properties to have an Idea on what happens when simulating a case numerically. Using all above, this thesis aims at determining which how COVID is diffusing from one infected human to a exposed one, under specific airflow rate conditions in a ceiling-ceiling ventilation systems. To perform this, we will create a complete model of the room and try to approach reality in terms of n2o concentration by comparing data with another experimental comparative thesis realized by another student. This study may validate our own model then it will be usable to look at contaminants in the whole room while experiments can only describes them at few measurements points. ANSYS workbench will be used in this thesis with Design Modeler for geometry, ANSYS meshing for meshes, ANSYS Fluent for simulations and CFD-post for post-processing.

The thesis report will proceed the same way as the protocol employed. After finding out relevant theory we will detail each part of the method to construct our model, then disseminate results and explain phenomena we will note at the end of this work.

4 Theory

4.1 Governing equations

In this study, there are several governing equations among which physics phenomenon are described as diffusion, advection, convection, conduction, radiation and chemical reactions. These equations are presented below and most of them are taken from ANSYS theory guide [6].

4.1.1 Continuity equation

The mass-conservation, or continuity equation, takes the form :

$$\frac{\partial \rho}{\partial x} + \nabla(\rho u) = 0$$

Being ρ the density of the air, u the incoming velocity. The equation depicts the mass conservation on each fluid element: the mass flow rates on each surfaces of a 3D cell are equal.

4.1.2 Navier-Stokes equation

For incompressible Newtonian fluids with constant properties, the Navier-Stokes equation is given by :

$$\frac{\partial u}{\partial t} + (u.\nabla)u - \nu\nabla^2 u = -\frac{1}{\rho}\nabla p + g$$

where :

$\frac{\partial u}{\partial t}$ is the time variation term

$(u.\nabla)u$ is the convective term

$-\nu\nabla^2$ is the diffusion term

$-\frac{1}{\rho}\nabla p + g$ is the source term

Moreover, this is a 3D equation then u, g and ∇ are vectors in the x, y and z directions.

4.1.3 Energy equation

For enery equation, four main terms are involved in change of energy in a fluid particle :

$$\frac{\partial(\rho E)}{\partial t} + \nabla.(u(\rho E + p)) = \nabla(k_{eff}\nabla T - \sum_i h_i J_i + \tau_{eff}u) + S$$

where the three terms in the bracket on the right-hand side of the equation represent conduction, species diffusion, and viscous dissipation, respectively.

The coefficient k is the conductivity k + k_t where k_t is the turbulent thermal conductivity.

J_i is the diffusion flux and S is the production term for volumetric heat sources [43] and radiation source term.

4.1.4 Buoyancy driven flow (or natural convection) and density model

As presented in the introduction, the exhaled jet of the manikin is distracted by natural convection and buoyancy due to thermal plumes (manikins), heaters (lights) and air supplies providing cold air in a hot room: $T_{supply} < T_{room}$. To consider these phenomena in the CFD simulations, we have to take into account the fact that the density of air in the room will change due to the temperature evolution. Two main density models can be used in such a configuration: the well-known Bousinessq model or the incompressible ideal gas law model. The first one is often used

because it allows accurate results in indoor environment problem since it is a model valid for low temperature variations. Moreover, its main advantage lies in the fact that it is not as time-consuming as the other model quote. Indeed, the Bousinessq approximation is a simplification of the incompressible model. It states that the density variation is only important in the buoyancy term, and can be neglected in the rest of the equation. This leads to the following relative variation of density

$$\rho - \rho_{op} = -\rho_{op}\beta(T - T_{op})$$

where T_{op}, ρ_{op} are respectively operating temperature and density, and β is the coefficient of thermal expansion which describes the relative increase in volume of a system when only temperature is varied.

However, we cannot use this model in this study because it is not compatible with the species transport model. Consequently, the incompressible ideal gas law assumption has been used in the whole thesis.

It depicts the density of a gas according to the following formula:

$$\rho = \frac{p_{op}}{\frac{R}{M}T}$$

R being the universal constant of gas and M the molecular weight of the gas.

4.1.5 Species transport

Mixing and transport of chemical species can be modeled in ANSYS Fluent, where the local mass fraction Y_i is calculated for species i . Both convection, diffusion, and reaction are described in this model. The conservation equation is the following:

$$\frac{\partial(\rho Y_i)}{\partial t} + \nabla.(\rho u Y_i) = -\nabla.J_i + R_i + S_i$$

where R_i is the rate of production of species by chemical reactions, S_i is the source of creation, J_i is the diffusion flux of species. This diffusion arises due to gradients of temperature and concentration. When no reactions are present, as for the case with a transport of N_2O in a room (used in this thesis), R_i becomes zero.

Then, we have the final equation :

$$\frac{\partial(\rho Y_i)}{\partial t} + \nabla.(\rho u Y_i) = -\nabla.J_i + S_i$$

4.1.6 Radiation model

Radiation model is used in few indoor environment problems since it is a useful model for high difference temperature cases. In our case the max difference is located at the surface of manikins, 34°C, compared to the averaged room temperature (22-23°C). However, at this surface convection is most significant physical phenomenon. Globally, in the room there is few differences in temperature which is due to temperature stratification over height but vary of only few degrees.

We will still compared data with and without Discrete Ordinates radiation model but there is no need to detail the theory part here since we just need to check that radiation model has no interest in the case of htis study.

4.1.7 Boundary conditions

Each model requires specific boundary conditions at some locations. In order to be understandable, we will categorize each boundary condition type regarding the different locations and parts of the room. They are summarized in the following table:

Inlets	Outlets	Manikins	Walls	Lights
u_i	p_o	T_m	$u = 0$ (no-slip)	T_{lights}
I_i	I_o	Y_i	$Q = 0$ (adiabatic)	
D_{hi}	D_{ho}	$D_{h,mouth}$		
T_{supply}		I_{mouth}		
		u_{mouth}		

Radiation boundary conditions can eventually be added in this table. Nonetheless, according to Menchaca-Brandan et al. [7], the internal emissivity for typical office surfaces is above 0.9. Then, this parameter can be unchanged and set to 1. Indeed, since the radiation model is not the most significant model in this thesis, it is not relevant to search for more accurate emissivities.

The BC for inlets can also be defined by the mass flow. Here, air flows through constant surfaces and we can use the inlet velocity as an input parameter. Outlets are set with a gauge pressure which can be measured during experiments. We often consider this pressure equals 0 since outflows have a lower velocity. For turbulence model, BC change according to which model we use. However, two different kinds of BC are mostly employed: k and ϵ values or I and another parameter. In our case, the hydraulic diameter, D_h, of the inlets will be added to the BC.

The last significant BC is the one linked to the energy equation. Either temperature or heat flux can be considered. By adapting to the numerous literature reviews dealing with thermal plumes of manikins in indoor environment, we will use temperature BC in the study.

Nevertheless, if almost every BC presented before are deduced from literature reviews or experiments, the inlet and outlet BC for the turbulence model must be defined: both the turbulence intensity and the hydraulic diameter must be found thanks to the following theory part.

4.2 Turbulence modelling

In turbulent flow the dependent variables (velocity, pressure and temperature) are not constant in time but vary in a stochastic way. Usually we are not interested in the precise time variation of all variables. Thus the dependent variables are split into a time averaged (mean) value and a turbulent fluctuation:

$$u = \overline{u} + u_{prime},$$

where u is the instantaneous velocity, and u is the mean value. The fluctuating velocity, u_{prime} , is defined by the difference between the instantaneous and mean velocity, $u_{prime} = u - \overline{u}$.

To define the turbulent viscosity, we need to come back to laminar flow equations. As an example, we will use the velocity component in the x-direction. Applying Newton's law to a fluid element, we get:

$$\rho u \frac{\partial u}{\partial x} = f$$

with f, the force per unit volume in the x direction.

To find f, we consider forces acting on the fluid in the control volume (figure 2). Two stresses exist: friction shear stress and pressure. Pressure difference has influence on the fluid element and can be assimilate to the pressure gradient (only valid for an element of fluid), $-\frac{\partial p}{\partial x}$. In a same way, shear stress is characterized by $\frac{\partial \tau}{\partial y}$.

For a Newtonian fluid, the shear stress is proportional to the velocity gradient :

$$\tau = \mu \frac{\partial u}{\partial y}$$

The shear stress gradient is :

$$\frac{\partial \tau}{\partial y} = \mu \frac{\partial^2 u}{\partial y^2}$$

We rewrite the the Newton's law using the previous equation, which gives :

$$\rho u \frac{\partial u}{\partial x} = -\frac{\partial p}{\partial x} + \mu \frac{\partial^2 u}{\partial y^2}$$

In a boundary layer the velocity in the y-direction has to be taken into account since a significant vertical (y-direction) velocity gradient appear due to walls. An acceleration term must be added to the Newton's law to model the boundary layer in this equation :

$$\rho u \frac{\partial u}{\partial x} + \rho v \frac{\partial u}{\partial y} = -\frac{\partial p}{\partial x} + \mu \frac{\partial^2 u}{\partial y^2}$$
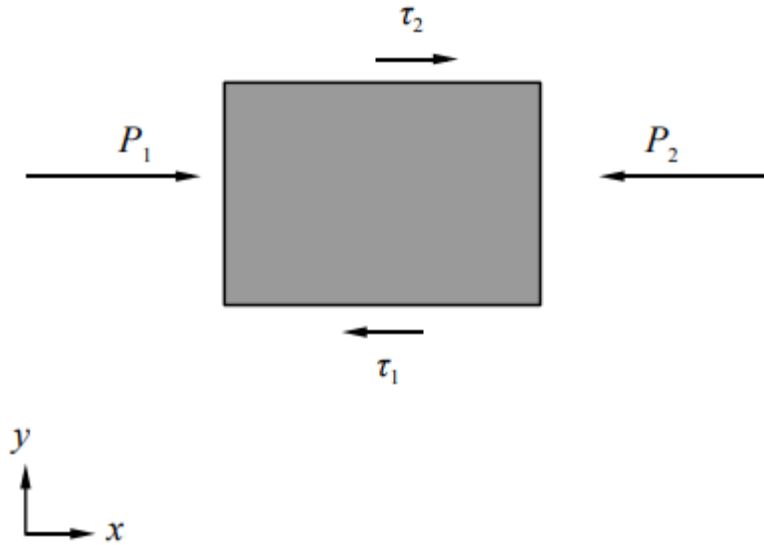
Figure 2: Control volume of a fluid element

Turbulent viscosity

We insert the turbulent dependent variables in x and y directions, respectively, $u = \overline{u} + u'$ and $v = \overline{v} + v'$. We finally obtain an equation for the time-averaged velocity :

$$\rho\overline{u}\frac{\partial\overline{u}}{\partial x} + \rho\overline{v}\frac{\partial\overline{u}}{\partial y} = -\frac{\partial\overline{p}}{\partial x} + \mu\frac{\partial^2\overline{u}}{\partial y^2} - \frac{\partial(\rho\overline{u'v'})}{\partial y}$$

where $\rho\overline{u'v'}$ is the turbulent Reynolds shear stress and the corresponding term in the right side of the equation can be seen as a force due to the fluctuating velocities u' and v'. However, the turbulent shear stress in previous equation is unknown since we don't have access to the precise time variation of all variables and especially velocity. This shear stress needs to be modelled : it is called a turbulence model. Usually, we model this stress by using a turbulent viscosity (or eddy viscosity) μ_t.

In order to be coherent with what happens in the well-known laminar case, we define the eddy viscosity as the ratio between the turbulent Reynolds shear stress and the vertical velocity gradient :

$$\rho\overline{u'v'} = -\mu_t\frac{\partial\overline{u}}{\partial y}$$

The sign "-" is due to the fact that the turbulent shear stress and the velocity gradient have almost always opposite signs. It will not be demonstrated in this thesis.

4.2.1 Turbulence models for indoor environment

Overview of turbulence models

Numerous literature review on indoor environment states the choice of the turbulent model is one of the main step of such a CFD study. A complete review of models used in predicting airflow and turbulence for indoor environment problems was performed by Liu and al. [9]. It shows a summary of all relevant CFD studies with the main models used, especially the turbulence models and their corresponding near wall treatment function. Radiation model is also stated. It takes in consideration the kind of ventilation system and the main objective of the study (the parameter measured). If this document do help to choose a pertinent turbulence model, it is not sufficient. Indeed, a lot of reviews underline that each CFD study, with its own particular characteristics (size

of the room, sizes and locations of inlets and outlets, known boundary conditions, mesh...), need a comparative study between several turbulence models usually used in enclosed environments. An investigation of turbulence models for HVAC systems is therefore important and different scenari may lead to different turbulent models even if they are really close from each other.

That is why we discussed what are the main turbulence models employed in indoor environment studies. As we will only use RANS models in this thesis, we will not consider other models linked to large-eddy simulation (LES) and direct numerical simulation (DNS). The most common turbulence models for room ventilation are the $k - \epsilon$, the $k - \omega$ and the Reynolds stress models (RSM). Additional near wall treatment is also considered. Furthermore, the $k - \epsilon$ model can be divided into three parts : the renormalized group (RNG) $k - \epsilon$, the realizable $k - \epsilon$ (RKE) and the standard $k - \epsilon$ (SKE) models. Concerning the $k - \omega$ model, the most used is the shear stress transport (SST) model.

A summary of most pertinent models in HVAC studies is presented below :
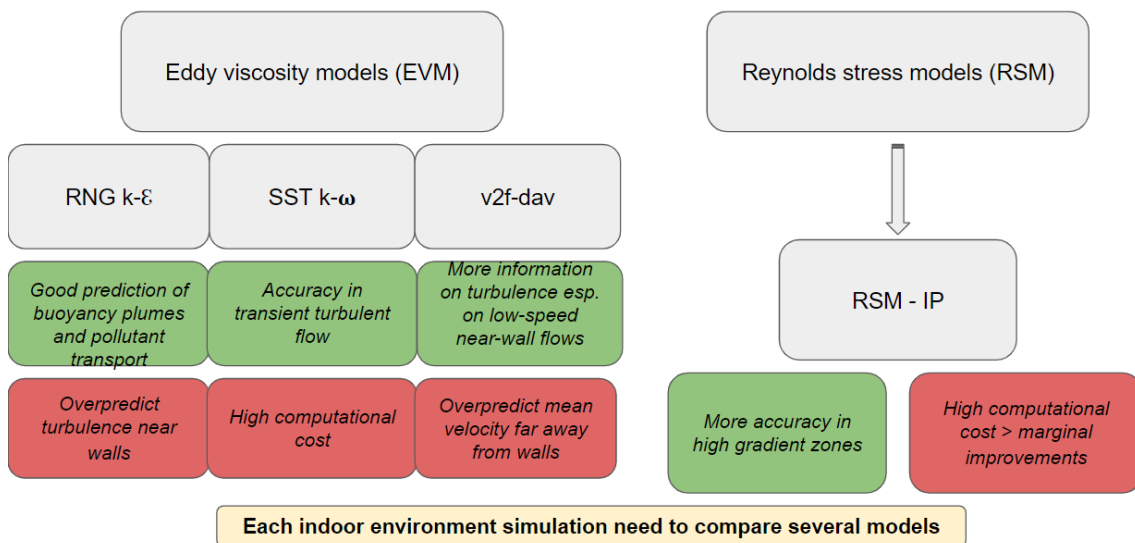

Figure 3: Turbulence models for indoor environment

After having studies several literature reviews, the $k - \epsilon$ model appears like the best one for our thesis. Indeed, it is the least computational costing and its main drawback is the overestimation of turbulence near walls, which is not a significant issue in our case since we are interested with tracer gas concentration around the infected manikins where turbulence is low.

Moreover, we can dismiss the v2f-dav model because it is not available in ANSYS fluent solver and it is rarely used in indoor environment simulations. RSM lead to time-consuming simulations and give marginal improvements. This model can be used if we require a high accuracy in high gradient zones. We do not aim at reaching such an accuracy as part of a master thesis.

Finally, we will compare the 2 turbulence models left, in the method part [ref] : the RNG $k - \epsilon$ and the SST $k - \omega$ models.

The $k - \epsilon$ model

As said in the turbulence modelling part above, a turbulence model is characterized by how the shear stress is modelled. The $k - \epsilon$ model belongs to eddy viscosity model (EVM) since the turbulent shear stress is only modelled using the eddy viscosity. This viscosity is obtained by solving two additional equations : one equation for the turbulent kinetic energy k, and one for its dissipation ϵ. Then, in this specific model, μ_t is obtained from these two parameters and the gas density. A dimensionless study shows the only way that ρ, k and ϵ can be combined to give the same dimension as μ_t is :

$$\mu_t = c_\mu \rho \frac{k^2}{\epsilon}$$

where c_μ is a constant.

The new element in the transport equations, compared to normal NS equations, is the sources and sinks. They are mainly dependent on velocity gradients, when the velocity gradients increase, k and ϵ increase too. In the previous definition of the turbulent viscosity, k squared appears then k increases faster than ϵ hence μ_t is larger in high gradient zones. That is why this model overpredicts turbulence near walls.

The $k - \omega$ model

This model is also an EVM. The difference with the previous one is that the transport equation for ϵ is replaced by an equation for the vorticity ω. The turbulent viscosity is calculated as :

$$\mu_t = \rho \frac{k}{\omega}$$

The SST model

The Shear Stress Transport model is an EVM which combines the k-ϵ and k-ω models. It adds a limitation of the shear stress in adverse pressure gradient zones to counterbalance the main drawback of the first model quote, namely high turbulence near walls. Then k-ω model is implemented in inner boundary layers while k-ϵ model in outer boundary layers.

4.2.2 Turbulence intensity

The turbulence intensity (I) is defined as

$$I = \frac{u'}{u}$$

Turbulence intensity is a significant parameter for simulating turbulent flow at the exit of pipes, especially around inlets and outlets in the case of the study. Since it is difficult to measure this parameter with accuracy, Russo and Basse [8] have documented the scaling behavior of the turbulence intensity with Reynolds number. The turbulence intensity over a pipe cross sectional area is :

$$I = 0.14 R_e^{-0.079}$$

where Reynolds number over a pipe of hydraulic diameter D_h is defined as :

$$R_e = \frac{u D_h}{\nu}$$

The hydraulic diameter is $D_h = \frac{4A}{P}$ where A is the cross-sectional area and P is the wetted perimeter. In our case, since inlets are cubic so this diameter is simplified : $D_h = \frac{4L^2}{(2L+2L)} = L$.

Then we obtain for the turbulence intensity at each inlet i, as we know the output velocity at inlets, u_i :

$$I = 0.14 \left(\frac{u_i D_{hi}}{\nu} \right)^{-0.079}$$

Where the dynamic viscosity ν has a value of 0.00001817 $[m^2/s]$ at the inlet temperature (21°C).

For turbulence intensity at outlets of hydraulic diameter D_{ho}, we need to realize a mass balance between inlets and outlets, considering that during the steady state the manikins are not breathing. We then have:

$$2u_o A_o = \sum_i u_i A_i \Leftrightarrow u_0 = \sum_i \frac{U_i A_i}{2}$$

where $A_i = 4L_i h_i$.

Finally,

$$I = 0,14 \sum_i \frac{u_i A_i D_{ho}}{2\nu}^{-0.079}$$

The calculations of turbulence intensity will be realized in the method part.

4.3   Mesh

4.3.1   Cutcell method

Two algorithms are available for assembly meshing: • CutCell • Tetrahedrons

CutCell meshing belongs to assembly meshing method designed for ANSYS Fluent. Both of these methods are quite similar since Tetrahedrons assembly meshing algorithm is a derivative of the CutCell algorithm. While the first one creates high quality unstructured mesh by combining the second one with other mesh manipulations, the Cutcell algorithm employes a patch independent volume meshing approach. It means surface mesh are created from input boundary pf volume mesh. Then, whether one uses a structured or an unstructured mesh, the CutCell method will be applied with respectively structured and unstructured meshes. This method is adapted for meshing containing single part bodies, which will be used in this thesis, and multibody parts. Structured meshes with hex cells give higher mesh quality than unstructured ones. Consequently, "the Cutcell algorithm often produces better results than tetrahedral methods" resulting in 80-95 % hex cell mesh. [10]

This algorithm follows 10 different steps and is a suitable method to correct poor mesh quality near sharp or rounded geometries (figure 4).

1. Size functions are defined.

2. A first grid is performed using the min and max cell sizes set up and extending to a larger domain than the defined geometry.

3. Limits of the geometry are considered and a uniform Cartesian grid is created within this geometry.

4. Specific cells with a lower size than those of the uniform grid are reworked and the corresponding grid is refined based on the local size.

5. A projection step is then applied to the mesh for the cells intersecting the geometry. The nodes are projected to the geometry (corners, edges, and faces).

6. After the previous step, the edges marked are either preserved or updated and used to build mesh faces. Once the mesh faces are constructed, cells are decomposed according to number of templates to recover these faces.

7. The mesh existing outside limits of the geometry is removed.

8. The quality of the cells thus generated at the border between the inside mesh and the deleted outside mesh is improved.

9. Cells are separated into cell zones. They are characterized by specific geometry property as cylinders in a squared rooms called virtual bodies. Bodies are treated by growing sizes then the smallest body is affected first to avoid mesh recovery issues.

10. Boundary conditions appear due to the cells zones, which consists of the neighboring cells between cells of one cell zone and cells of one another zone. These cells are recovered, especially cells of boundary conditions linked to named selections.

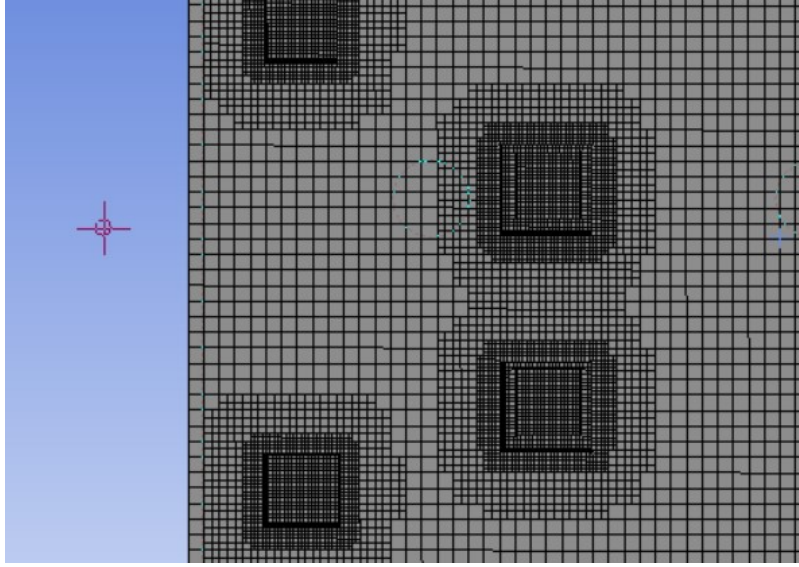Results of the Cutcell method are shown below with the final mesh created in this thesis :

Figure 4: Cutcell method

5 Method

5.1 Scenarios

One standing infected manikin is breathing in an enclosed environment and diffuse COVID in the room where another manikin is sitting. The infected manikin is breathing at normal human rate while we desactivate breathing for the exposed manikin. Indeed, it will create additional turbulence which is not particularly required since only n2o concentration near its mouth interests us and the spatial influence of breathing zone is short. The main influencing variables of contaminant concentration are the distance between manikins and airflow rate conditions. Then simulations will be realized under 3 different ACH for 1-meter distance case, namely 2.7, 5.1 and 9.6. Another simulation will be performed under 2.7 ACH with separated distance of 2 meters. Distance between manikins is set up as the distance from mouth to mouth.

Simulations will consist in 2 parts : steady and transient. As done experimentally in the comparative study, we will launch a steady simulation till room temperature reaches its steady state, a value around 22-23°C. After this step, we start a transient simulation incorporating n2o mass fraction and breathing function at the mouth of the infected manikin.

5.2 Experiment and equipment

5.2.1 Experiments

Despite this thesis does not aim at realizing experiments but simulations in correlation with previous experiments, Indeed, the most significant data was obtained in the parallel experimental thesis such as airflow rate measurements in the room, n2o tracer gas concentration and geometry data.

In particular, airflow rate distribution is useful. The supply air diffusors were balanced experimentally to deliver the same airflow rate. It has been measured through the pressure drop using a manometer. The airflow rate was calculated using the square root of the pressure drop multiplied by the k-factor. Each different supply has his own k-factor which is referenced by the constructor:

Name of unit	Type	k-factor
Orion-Opus 200-250	Supply units (SU_1, SU_2, SU_5)	26.8
Orion-Opus 125-160	Supply unit (SU_4)	12.4
Orion-Opus 250-315	Supply unit (SU_3)	36.7

Figure 5: k factor values

The following table shows the percentage of total airflow rate delivered by each supply :

Supply air diffuser	% of total airflow rate
SU_1	20.8
SU_2	17.6
SU_3	21.5
SU_4	17.8
SU_5	22.2

Figure 6: Percentage of airflow rate

In the experimental thesis, these values were measured to consider the supplies as balanced. In our thesis, we will use these values to obtain realistic boundary conditions at inlets. Nonetheless, no data was collected concerning exact locations and sizes of air supplies and lights, velocities at inlets and temperature of the lights of the room. The geometry measurements are presented in Method → Geometry and other data is shown in Method → Models.

5.2.2   Measuring equipment

Zamo laser

A Zamo laser device was used for geometry measurements to find out locations of inlets, outlets, lights and walls by using distances estimated from an origin fixed at a corner of the room. The accuracy when measuring distances is 3 mm which is far enough to evaluate a 6-meter room geometry.

Figure 7: Laser rangefinder

VELOCICALCPlus

Velocities at inlets was measured by a VELOCICALCPlus anemometer. The plane, defined by the measuring filament and the two bars protecting at the extremity of the rod, has to be positioned perpendicular to the axial velocity we want to measure. Then, we need to rotate 90° the rod to measure velocities in the y and z directions. We will see in the following that we only measured velocities in an horizontal plane around inlets. Thus, one measurement point requires one rotation. The accuracy of the device is 0.015 m/s which meets our expectations since range of mean velocities in the room is 0.2-0.7 m/s
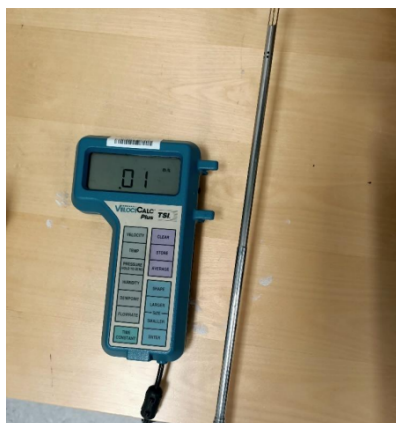

Figure 8: Anemometer

Autozeroing manometer

Autozeroing manometer TT-570 was employed to measure gauge pressure at outlets and check that airflow distribution between inlets is still the same as previously. One tube was exposed at the ambient pressure of the room whereas second tube was inserted in air vents.

Figure 9: Manomometer

5.3 Geometry

The laboratory room is considered here as a single part body. Every other bodies such as manikins, air supplies and lights will be considered as outer surfaces thanks to the Boolean operation which allows subtracting bodies from parts. Indeed, what happens inside air vents is not relevant in the case of this study and real flow cannot got inside both manikins and light walls.

5.3.1 Simplified geometry

5.3.2 Real geometry of the laboratory room

The room is modelled with a 3D geometry. Length L of the room is 6.2 m towards x-axis, width W is 4.7 m towards z-axis and height H is 3.05 m towards y-axis.
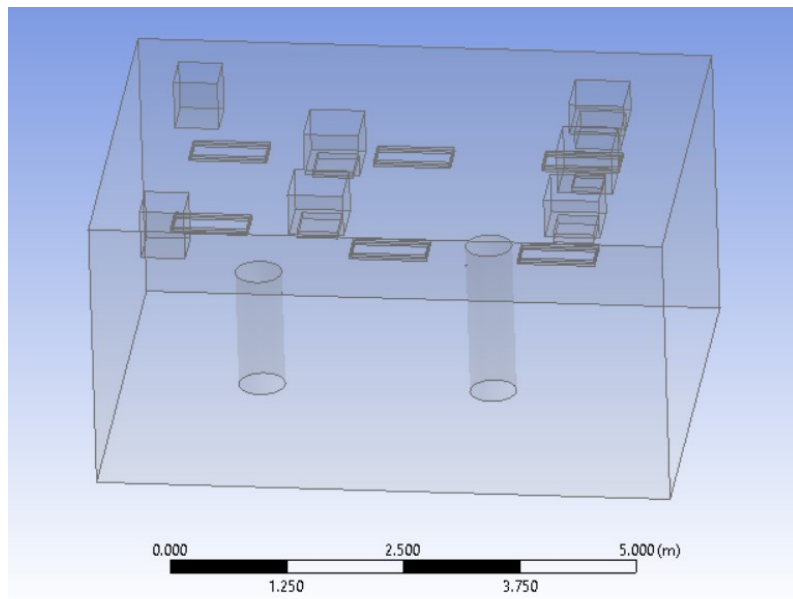
Figure 10: Room geometry-global view

Air supplies

Air supplies are constituted by 5 orion opus diffusers using swirl pattern. This kind of airflow pattern is complex and a modelling of these air vents will be required (see Method → Models → Inlets model).
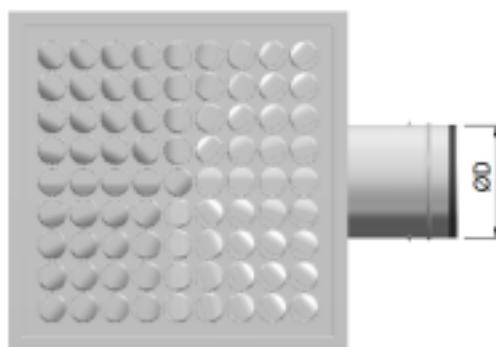

Figure 11: Orion opus diffuser

18

Every heights of inlets are in range 2.47-2.5 m. Other geometry data is shown in the following table :

Type	x[m]	z[m]
1a	2.33	2.64
1b	2.31	1.24
2a	5.11	3.39
2b	5.17	2.36
2c	5.14	1.4

Every inlets contain diffusors which describes a squared shape of length 0.435 m for inlets 1a, 1b and 2c, 0.325 for inlet 2b and 0.49 for inlet 2a. They will be considered as hydraulic diameters further in the study.

Manikins

Our model of manikins consists in cylinders of diameter 0.5 m and different heights for standing and sitting manikins. CFD manikin have been created following the same manikin as previously used in experimental set-ups at NTNU (Aganovic and Cao, 2019) and in the parallel master thesis. The height of the infected standing manikin (M_inf) was 175 cm and an assumed weight of 75 kg. The breathing zone was at 160 cm.

	M_{inf}	M_{exp}
Height	1.75	1.25
Diameter	0.5	0.5
Breathing zone	1.1	1.6
Mouth diameter	0.016	0.016

Lights

Lights lead to thermal diffusion in air. As in this study, lights are really close to inlets, it is interesting to consider them as heat source in order to examine if they can have influence on airflow entering the room.

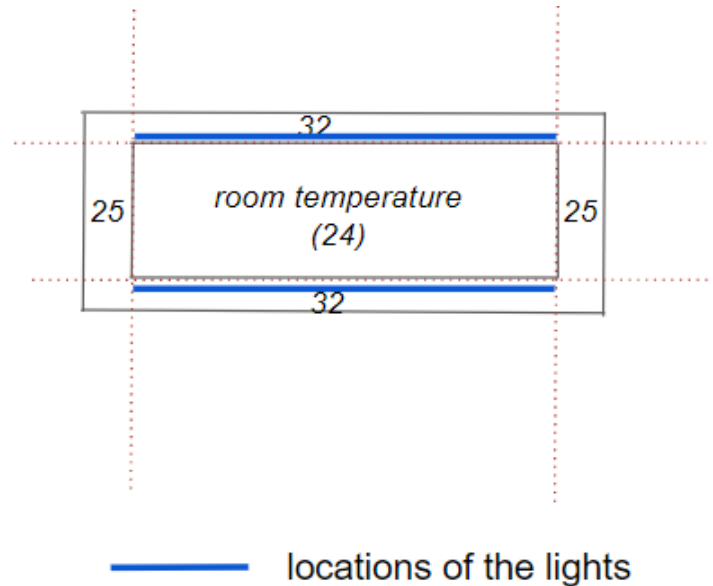Room lights are empty in the center and lights are on 2 sides of light walls :

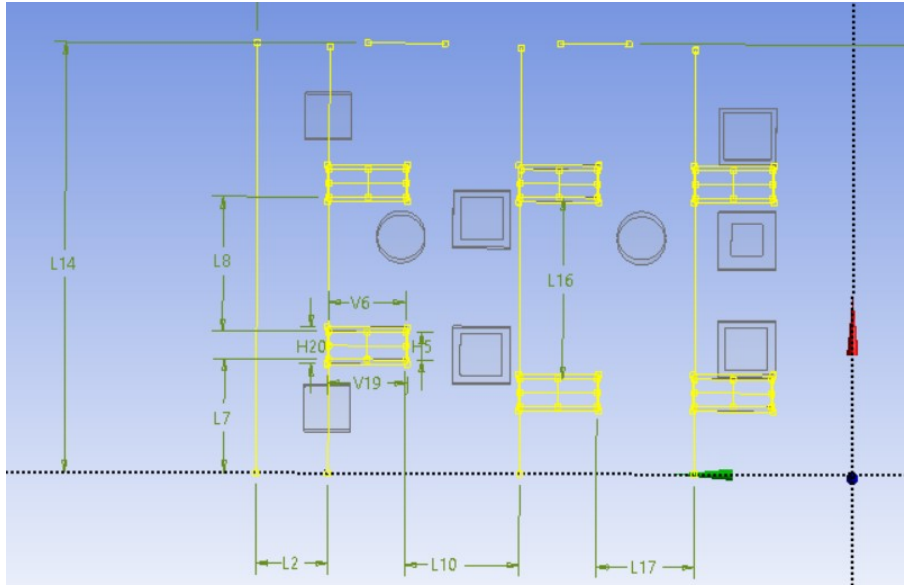Figure 12: Lights design

Locations of lights are presented below :

Figure 13: Lights locations

H20	0.382 m
H5	0.29 m
L1	6.2 m
L10	1.19 m
L13	4.47 m
L14	4.47 m
L16	1.88 m
L17	1.02 m
L2	0.75 m
L7	1.18 m
L8	1.4 m
V19	0.832 m
V6	0.8 m

Figure 14: Lights measurements

In the case of the study, we will not use CTM to model human bodies since it makes meshes and simulations much more complex and bigger. The main impact of not choosing such a model will be difference in thermal plume effects since surface body is less detailed in more simple models. Indeed, in a case of cylinders, thermal plume will be higher than in CTM case. In the cylinder model, there are no empty spaces at legs, arms, hands and surface body is continuous. Therefore, it will not exist discontinuities in thermal plume at surface of manikins. We must take this fact in consideration when discussing bout thermal plume effects.

5.4 Mesh

5.4.1 Simplified meshes

Before continuing with different circumstances of the laboratory room, meshing study of baseline scenario is strongly recommended to be implemented for obtain a more confident simulated result. Therefore, three simulations of the baseline model were generated as different number of cells. Not only global grid spacing changed but also local spacing in face sizing or inflation functions. This study aims at defining how the cells in high gradients regions, namely around manikins, lights and air supplies, must be refined. This preliminary work on a simplification of the real room geometry will allow to create rapidly a correct and efficient mesh on further study using a more complex mesh. That is why we achieve three different meshes, coarse, medium and fine mesh, all counting less than 1 million cells which represents less than 1 hour of calculations for the first simulations.

The quality of the mesh is however not sufficient to consider whether a mesh is suitable. We also need to look at y+ requirements in indoor environment and refine the mesh if it is necessary (ADD A Reference to the Y+ theory with range of y+ accord to turbulence models). Nonetheless, we have to take into account the number of cells of the final mesh we want because it is directly linked to the computational cost which can be several days for heavy calculations. For example, the first fine mesh created contained more than 5 million cells to reach a y-plus below 5 in order to use the enhanced wall treatment. For simulating one case in the transient mode to model the breathing of the manikin over time, it required at least 20 hours of continuous simulation with poor accuracy and convergence. That is why after the comparison of the three different meshes of the simplified room, we put a limit on the maximum cell number of 1.5 million.

The following comparison table was established according to mesh quality requirements, suggested by the ANSYS user's guide[10]. The two scales below show the requirements for two of the main quality parameters: skewness and orthogonal quality :

Excellent	Very good	Good	Acceptable	Bad	Unacceptable
0-0.25	0.25-0.50	0.50-0.80	0.80-0.94	0.95-0.97	0.98-1.00

Figure 15: Skewness scaling

Unacceptable	Bad	Acceptable	Good	Very good	Excellent
0-0.001	0.001-0.14	0.15-0.20	0.20-0.69	0.70-0.95	0.95-1.00

Figure 16: Orthogonal quality scaling

Moreover, ANSYS user's guide suggested limits values for both skewness and orthogonal quality. According to the previous scaling and theory, cells will be considered well constructed when their skewness are lower than S_max and their orthogonal quality are higher than OQ_min. Every cells which do not respect these requirements will be manually refined till they reached acceptable values.

The requirements are the following :

$S_max > 0.95$

$OQ_min < 0.1$

These limits are the limits when one cell may lead to divergence in simulations. For more comfortable computation, we will consider groups of more than 10 problematic cells with skewness above 0.80 and orthogonal quality below 0.15.

Then, in adequacy with the previous scaling, we create the following comparison table using three meshes with different number of cells, to determine which face sizing and mesh manipulations have to be done so that we can obtain satisfying mesh metric parameters. Despite it has been realised with unstructured meshes, it is still useful to construct structured mesh since issues in mesh quality often comes from problematic boundaries as inlets or manikins.

Face sizing must be operated for boundary face of supply air diffusers (Air Inlet) and Exhaust Grilles (Air Outlet). In the baseline cases, four different kinds of locations were applied as specified face sizing: air inlet faces, air outlet faces, exterior walls and lights. Since air temperature and velocity are changed significantly at these locations, quality of mesh at these locations required higher than the rest according to literature review and our knowledge in fluid mechanics. This table will be useful to determine what the parameter of the face sizing must be.

Quality of mesh	Coarse	Medium	Fine
Number of cells	145260	373850	782995
Aspect ratio (*avg*/max)	*1.878* / 9.752	*1.866* / 26.838	*1.815* / 6.284
Orthogonal quality	*0.7504* / 0.9883	*0.7538* / 0.9918	*0.7754* / 0.9950
Skewness	*0.2484* / 0.9534	*0.2451* / 0.9830	*0.2238* / 0.7424
Computational cost (1000 ite)	*6-7 min*	*20 min 30 s*	*50 min*

Figure 17: Comparison table of 3 different simplified meshes

The fine mesh case gives correct values (which will be improved in structured meshes) then the following face sizing will be used as baseline parameter for further more realistic meshes of the room considered in this thesis :

- 20 mm for manikins face sizing

- 25 mm for inlet and outlet boundaries

- 30 mm for light walls

- 4 mm for manikins' mouths

5.4.2 Meshing method

"Mesh" from ANSYS workbench was employed for meshing to case of ANSYS Fluent with its efficient and high-quality characteristics. In this project, default grid spacing is set as 0.120 m for global sizing of our 6-meter room with a max size length of 0.300m. Indeed, both 0.100m horizontal spacing and 0.300m vertical spacing are advised for common office room (size of 5 m), and we could see that decreasing this global spacing does not affect significantly the quality of the mesh. Moreover, requirements for any CFD study of indoor environment using RANS models exist [5]. Indeed, the number of cells N for standard CFD using 2-equation turbulence modelling with wall functions must respect a minimum value:

$N_{min} = 44400 * V_room^{0.38}$

where $V_room = L * l * H = 6.2 * 4.7 * 3.05 = 84.53m^3$

Finally we have : $N_{min} = 239689 cells$.

In this study, we are using hex dominant structured grid with the CutCell function (i.e. theory part, meshing) even if we have also studies tetrahedral unstructured grid with prism boundary layer. Figure X shows the generated mesh of the laboratory room, where the right figure is zoom-in of the top corner of the left figure. Not only global sizing can be restricted in ANSYS mesh, but

size of face and inflation can be specified. In the areas with large changing of fluid properties, the higher of the mesh quality, the more accurate of the obtained results. In ANSYS mesh, intensive mesh at areas of manikins, air inlets, air outlets, exterior walls have been generated since both air temperature and velocity changed significant at these places. The meshing outcome produced by ANSYS mesh of the room as figures below:
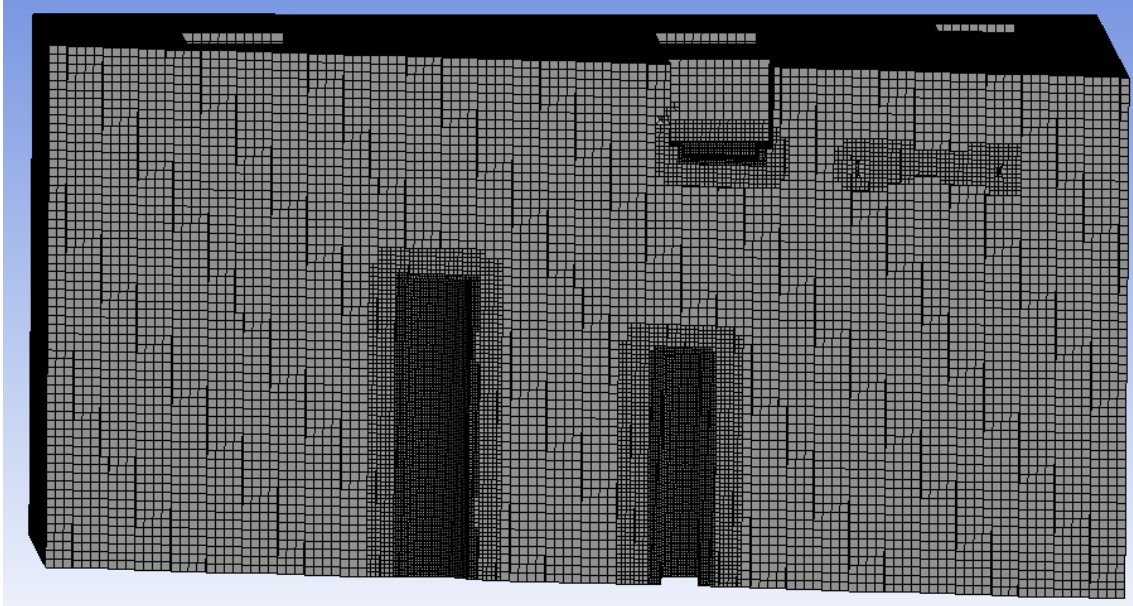

Figure 18: Structured mesh

The techniques and grid spacing can then be used for the real room geometry in order to obtain a quality mesh. Further simulations with this mesh will lead to some improvements and y+ adaptations. Especially, when we try first to launch transient simulation, we could note we need to use a time step over 0.1s for one simulation to be feasible in less than one day. However, it was really hard for the solution to converge and even diverged for time steps close to 0.5s. With an unstructured grid and high time steps in terms of the CFD condition (cf CFL) (Δ_t ¿ 0.1s in our thesis) the solution may meet a floating point leading to divergence. This point comes from a significant size difference of two neighbors' cells so equations like the mass flow conservation between the two cells is not possible anymore and results diverge toward infinite values. Consequently, we decided to use in parallel a structured grid to compare and to get better accuracy. We finally have the following mesh quality:

	Unstructured mesh	Structured mesh
Number of cells	1 004 934	952 638
Skewness (avg/max)	0,20957	1,35e-002
Orthogonal quality	0,78935	0,97985
Aspect ratio	2,3842	0,99273

Figure 19: Comparative table of unstructured and structured meshes

We can note the structured mesh has a far better quality than the unstructured one. It will lead to faster calculations for same convergence and will avoid floating point. For the end of the study, we will then the structured mesh for every simulation.

Maximum values of skewness have been studied so that divergence cannot happen. According to ANSYS suggestions, we target the mesh locations where the skewness was lower than 0.80, which is considered as the limit of acceptable values. We refine each location where at least 10 close

cells, which can be sufficient to make the solution diverge, have a skewness higher than this value. We then check with other mesh quality parameter to be certain no nodes can lead to some issues during the simulation.

5.5 Inlet velocities modelling

Assumption for modelling the real air supply of the laboratory room

It is really complicated to copy every single hole in the air supply system because, contrary to some other devices having a similar design, the supplies here are quite different. They have been designed to be experimental first that is why there is no obvious link between two holes of one air supply. Then it becomes hard to create an accurate algorithm to determine the direction of the airflow at each hole. Another solution would have been to directly measure each direction for each hole. However, supplies count for more than 300 holes. Consequently, instead of losing a lot of time to find an efficient and accurate way to measure all the directions, it seemed more judicious to model in an easier way the 5 inlet supplies.

Bacis of the model

As the manikins are far enough from the inlets (more than 1 m), it can be considered that it is not necessary to have the exact direction of the airflow coming from each single hole. It is more relevant to have the main behavior of the flow around inlets in the horizontal plane as we assume the vertical direction can be neglected compared to the horizontal one.

In order to do this, we measure velocity of the flow at 8 different points for each inlet in x and y direction, hence 40 measurement points (80 velocities to be measured) in a horizontal plane since vertical velocity can be neglected against horizontal one. Velocity measurements on inlet 1a showed that vertical velocity was at least 10 times lower than horizontal velocity. That is why we do not need a 3D model for inlets but only 2D surfaces is enough accurate to model air vents. Measurement points are located around inlets at the borders and the upper extremity of the anemometer rod is fixed with the lower surface of inlets where flow enters the room so that every measurement are performed at same height to collect more pertinent data.
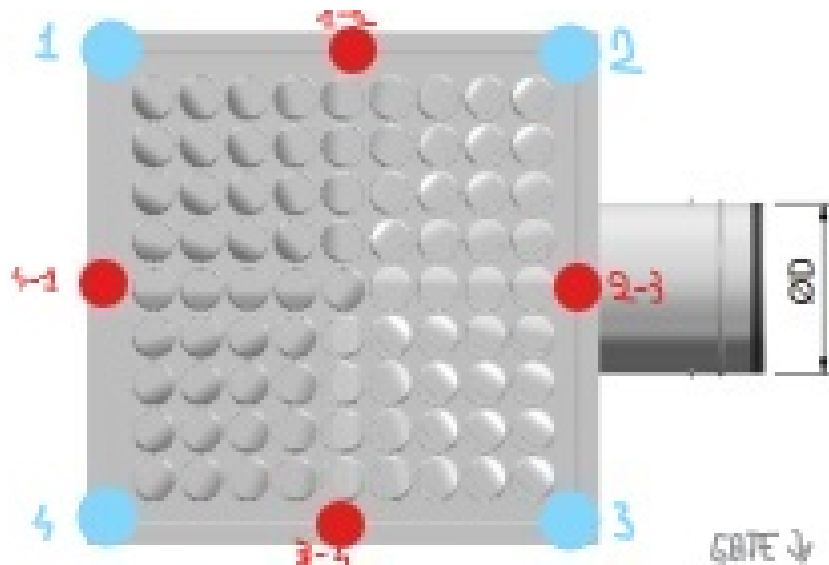
Measurement points are shown below :

Figure 20: Measurement points

Then, we creates a vertical extrusion assuming there is no vertical velocity variation from what has been said before. Each of four surfaces has a normal inlet velocity as boundary condition. Therefore, combining the vertical extrusion with velocity normal to surface of this extrusion allows modelling horizontal velocities at exits of the diffusors. One of the main advantage of this model is that, even if vertical velocity is not measured, it still depicts a vertical diffusion as the velocity will be applied on a little height h as the surface of the extrusion is defined by height h and width w.

Consequently, knowing ACH, we can, after measuring velocity, deduce the surface of each rectangle of the extrusion and then the height of these rectangles to be modeled on ANSYS Fluent.

The velocity measurements were realized at an ambient room temperature of 24 degrees C, relative humidity of 20% and with a total airflow rate in the room of 640 m^3/h corresponding to 7.6 ACH. Measurements are performed in the plane shown in the following figure, corresponding to a horizontal plane in the 3D geometry room. Each measurement point contains two values: second one is velocity measured in direction defined by the axis of the supply duct in the right part of the figure while first one is perpendicular to this axis.

Measurement location	Inlet 1a	Inlet 1b	Inlet 2a	Inlet 2b	Inlet 2c
1	0.10 | 0.46	0.11 | 0.38	0.03 | 0.17	0.25 | 0.95	0.09 | 0.60
2	0.10 | 0.51	0.26 | 0.09	0.15 | 0.04	0.75 | 0.17	0.62 | 0.10
3	0.20 | 0.26	0.15 | 0.30	0.24 | 0.10	0.14 | 0.72	0.40 | 0.06
4	0.42 | 0.10	0.34 | 0.09	0.15 | 0.04	0.54 | 0.15	0.45 | 0.10
1_2	0.42 | 0.20	0.36 | 0.20	0.11 | 0.14	0.68 | 0.15	0.25 | 0.22
2_3	0.25 | 0.27	0.28 | 0.35	0.12 | 0.09	0.17 | 0.56	0.24 | 0.22
3_4	0.36 | 0.20	0.30 | 0.16	0.07 | 0.12	0.62 | 0.28	0.43 | 0.17
4_1	0.16 | 0.42	0.18 | 0.32	0.18 | 0.07	0.22 | 0.92	0.15 | 0.27

Figure 21: Velocity measurements

The value of airflow rate used in these measurements has no importance. Indeed, we only use it with final velocity to find out effective height of the extrusion of inlets then recalculate new velocities for each of the three considered airflow rates (i.e. ACH of 2.7, 5.1 and 9.6).

Effective height calculations

Knowing flow velocity at inlets and airflow rate, we can finally determine the effective height h for each inlet. We average the normal velocity on each face. Consequently, airflow rate Q_{face} through one vertical face j of one inlet i with dimensions w_i, h_i is:

$$Q_{i,j} = U_{avg,i,j} * w_{i,j} * h_{i,j}$$

Then, airflow rate delivered by one inlet is :

$$Q_i = \sum_j U_{avg,i,j} * w_{i,j} * h_{i,j}$$

$$Q_i = 4 * U_{avg,i} * w_i * h_i$$

where

$$U_{avg,i} = \frac{1}{4} \sum_j U_{avg,i,j}$$

Then, we have :

$$h_i = Q_i/(4 * U_{avg,i} * w_i)$$

To calculate the averaged velocity on each face from the measurement points (illustrated as red points), we divide each face in 4 four different parts as shown below:
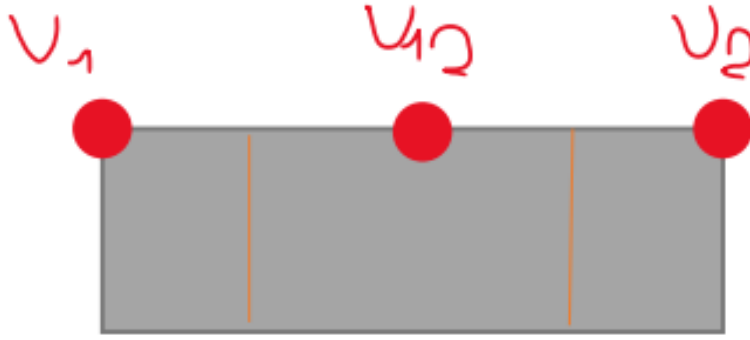
26

Figure 22: Vertical face division

Velocities are measured on the upper segment since vertical velocity variation is neglected. We proceed in a linear way to estimate averaged output velocity from velocity measurements:

$$U_{avg,i,j} = \frac{u(1) + u(2)}{4} + \frac{u(12)}{2}$$

From all the steps before and $h_i = Q_i/(4 * U_{avg,i} * w_i)$, we compute effective height for every inlets :

	inlet 1a	inlet 1b	inlet 2a	inlet 2b	inlet 2c
h_i	0.067	0.076	0.203	0.050	0.104

Averaged velocities for different ACH

Now that we have effective heights, we must proceed the opposite way than before. From effective heights and airflow rate of each inlet, we calculate the averaged velocity for each inlet. The following velocities will be used as inlet boundary conditions for simulations (see Method → Models → Boundary conditions) :

ACH	Airflow rate	Uavg,inlet1a	Uavg,inlet1b	Uavg,inlet2a	Uavg,inlet2b	Uavg,inlet2c
2,7	226	0,112	0,083	0,034	0,172	0,077
5,1	430	0,214	0,159	0,065	0,328	0,146
9,6	810	0,403	0,299	0,122	0,617	0,275

Figure 23: Averaged velocities for inlets

Vertical velocity justification

Vertical velocities could have been measured to make the model finer. However, due to the difficulty to fix a constant height for vertical measurements, experiments would have been realized with less accuracy. It is not coherent to add extra experimental data in a CFD study if we cannot reach accuracy we want, especially when this data can be neglected against other measured data. It is better to create a model with data we master, been measured in a more confident way.

Furthermore, adding such measurements represents 8 more points to consider for each inlets which means 40 extra measurements points. This is why, it is relevant to ponder about the real interest of such data.

In spite of what we have just said, it is required in such a study that we validate the model previously established with experimental data. If this latter data is far from data we will obtain with inlets model, we may need to measure additional data like vertical velocity.

5.6 Breathing mode

Species transport model was combined with a breathing mode in order to simulate emission of Covid-19 particles. We considered here one main breathing mode: normal breathing. For this mode, we try to approach the experimental exhaled velocity as shown below, inspired from Rencken et al. [12]:
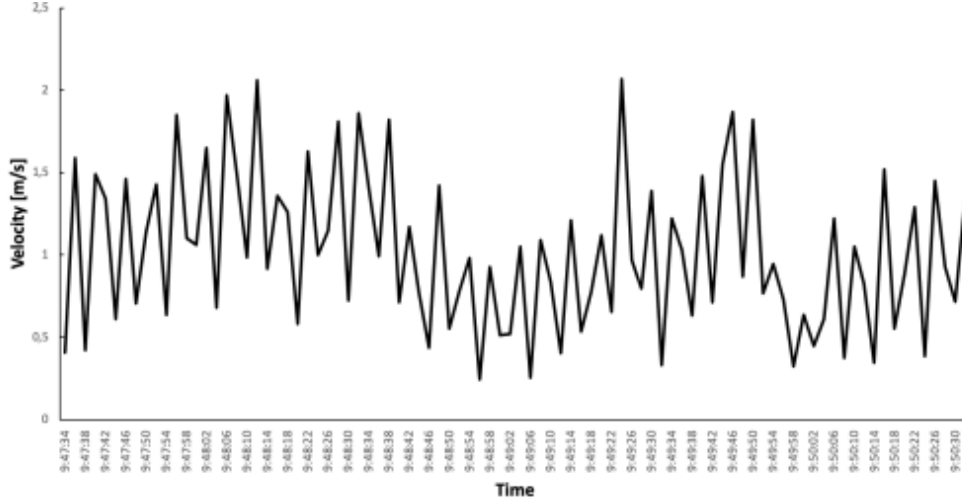

Figure 24: Experimental breathing mode

A sinusoidal function is a good way to model the previous breathing function. We know from the corresponding experiment that the averaged velocity is 1.5 m/s through the mouth of the manikin, being a tube of diameter 0.016 m. As we modelled in our study the mouth by a square surface (edge length l of 0.016), we need to recalculate the averaged velocity for our study.

We must have in both cases the same experimental and theoretical airflow rates, respectively Q_{exp} and Q_{th}. In the comparative experimental study, human adult breathing are normally 12 breaths per minute, which means 5 second period of one breath (Johns Hopkins Medicine). This means an airflow rate of 22 L/min.

Then, the theoretical averaged velocity is :

$$U_{avg,th} = \frac{Q_{exp}}{l^2} = \frac{Q_{th}}{l^2}$$

$$U_{avg,th} = \frac{22}{1000 * 60 * (0.256)^2} = 1.43 m/s$$

Finally, inlet velocity at the mouth of the infected person has an averaged velocity of 1.43 m/s and our corresponding sinusoidal function is :

$$1.43 * [sin(\frac{2\pi}{5}t + 1]$$

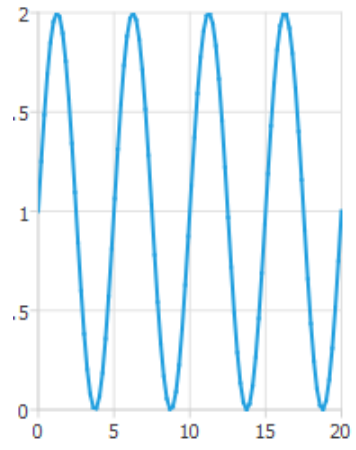Then, after realizing simulation in steady state mode, we launch a transient simulation with the following velocity:

Figure 25: Breathing function

5.7 Numerical setup

5.7.1 Model selection

General

In general setting, the gravitational acceleration is -9.81m/s2. Cases in this project are simulated as steady state thermal analysis firstly, then they are combined with transient model to simulate breathing modes of the infected manikin which are not constant in time. Energy model was turned on since temperature distribution act as a very important factor for consideration of indoor thermal comfort.

The following air properties are considered at a temperature of 21°C which is the temperature of air entering the room :
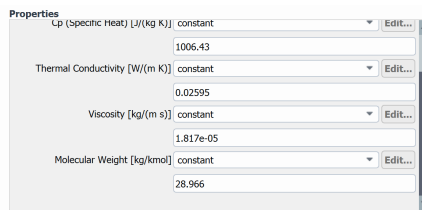
Figure 26: Air properties

Turbulence

The RNG k-epsilon model was selected for viscous model in ANSYS Fluent. From the theory part, we deduce only 2 main different turbulence models : the RNG $k - \epsilon$ and the SST $k - \omega$ models. To determine whether it is interesting to use either the first or the second model, we plot the velocity against height of the room at middle distance of the two manikins which is the zone that we will focus on. The results are shown in the following graphic.
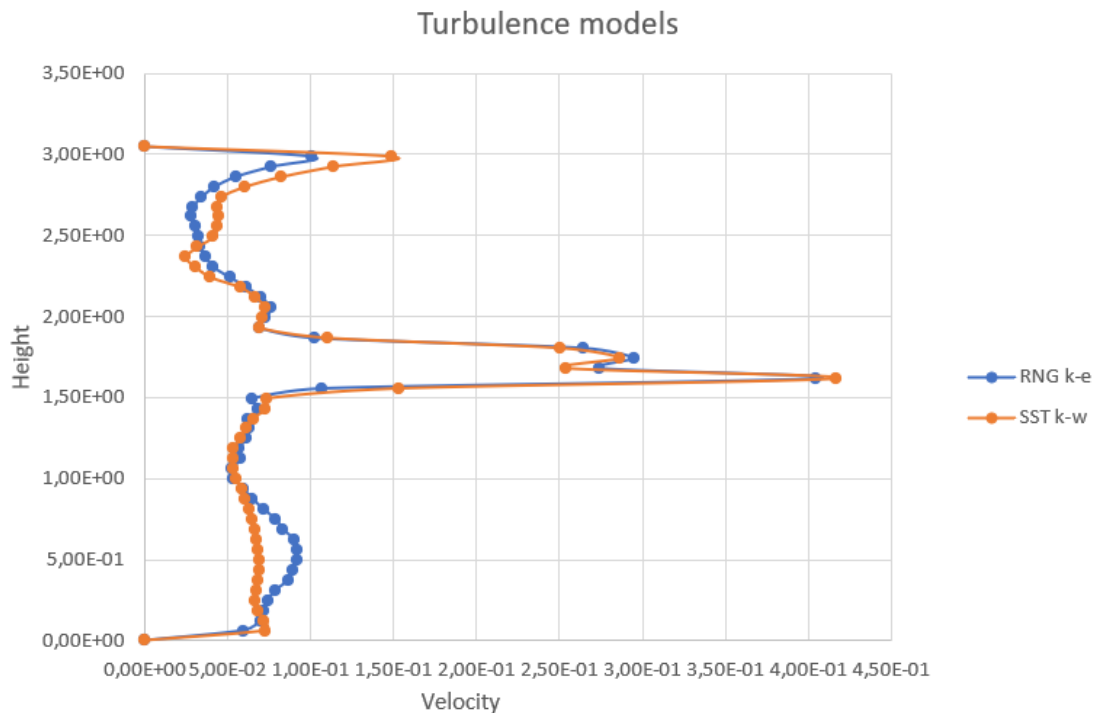
Figure 27: Comparison between turbulence models

As expected, the $k - \epsilon$ model overestimates the turbulence near walls resulting in higher velocity near the room floor. However, we only have a little difference between velocities obtained from the 2 models and velocities in the breathing zone is (1.5 to 1.9 m) are quite similar with a percentage relative difference lower than 5%. Therefore, our thesis does not worth to use the SST $k - \omega$ model which is more computational costing. That is why we finally choose the RNG $k - \epsilon$ model for the whole study.

The near wall treatment with scalable wall function was applied for case of ANSYS. Indeed, near wall there exists near wall treatment requirements for CFD. These requirements lead to different meshes estimating below (for a typical room with a 6-meter length) :

- y+ $\leq$ 11 for standard wall function (2 million cells)

- y+ $\leq$ 30 for scalable wall function (1 million cells)

- y+ $\leq$ 5 for enhanced wall treatment (5 million cells)

```
      sitting_manikin              9.9659537
     standing_manikin             10.466141
           wall-solid              7.7257743
         wall_ceiling             12.454183
           wall_floor             12.443801
          wall_lights              7.0466786
           wall_outer              9.5877835
```

Figure 28: Wall y+

In the case of this thesis, it is not interesting to use more than 1 million cells since we do not need such accuracy and time simulation will be too high with the available devices. Consequently, we will use scalable wall function in the whole study.

Full buoyancy effects have been chosen for additional option of viscous model since the gravity force and non-isothermal flow has effect to generation of turbulence kinetic energy because of buoyancy effect.

Furthermore, it exists a gate in the real room geometry, but this gate is formed of 2 different gates separated by a layer of isolation containing air. We can then assume the gate is at the same temperature than the side walls then there is no heat transfer from outside the room at its location.

Species transport

Covid-19 particles can be modelled in lots of different ways. In this thesis and to be loyal to the modelling of airborne transmission in the experimental thesis, we use a tracer gas. Tracer gas is used in several studies to mimic aerosols with diameter lower than 5 μm according to Ai and al. [12]

For normal breathing process, using tracer-gas diffusion analysis is reasonable since the number of droplets in the exhalation is almost zero. Simulating droplets transport by concentration conservation equation means shear stress, gravitational setting, and electrostatic force effect are not taken into account. In normal breathing, due to the same high velocity of droplets and the exhaled air and the fact that the momentum, heat, and mass exchanges between droplets and room air can be neglected. After this initial period the evaporation and cohesion phenomenon will be significant and aerodynamic investigations on droplets or particles are necessary. In this regard, the simulated tracer gas movement in this study will more closely represent the fine droplets, especially those with an aerodynamic diameter less than 5 μm. Modeling the movement of larger-size particles

31

requires the more complicated particle trajectory modeling approach, or the Eulerian approach taking into account the gravity settling effects (2nd step).

Therefore, three phenomena are not considered in this thesis : evaporation of large droplets, gravity settling affecting large drolets and intermediate droplets (5-100 5 μm) dispersion.
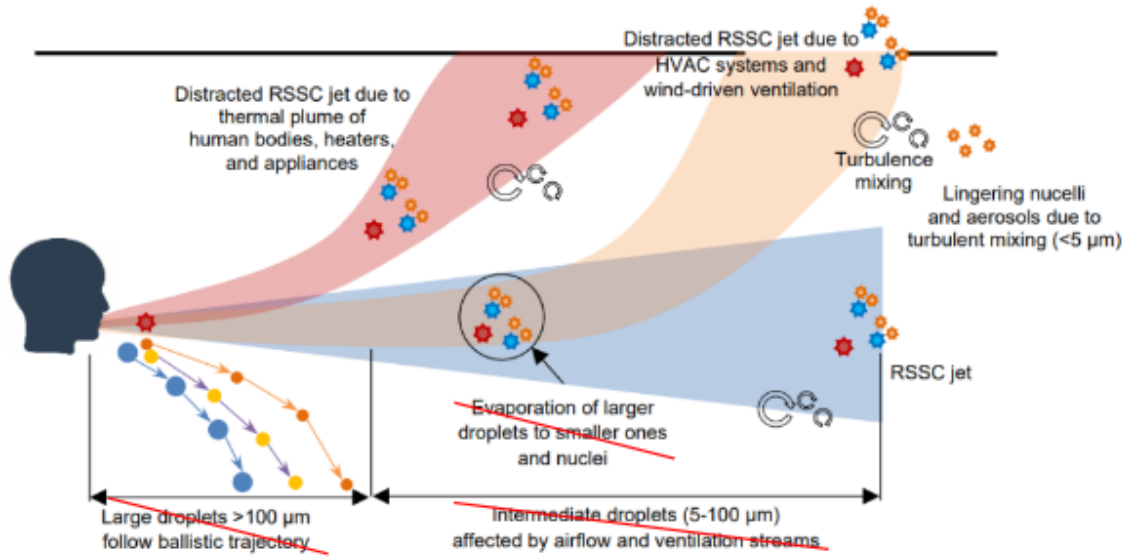

Figure 29: Comparison between turbulence models

5.7.2 Boundary conditions

Air inlet (velocity inlet)	**2.7 ACH**				
Velocity specification method	Magnitude, normal to boundary				
Temperature (C)	21				
	Inlet 1a	*Inlet 1b*	*Inlet 2a*	*Inlet 2b*	*Inlet 2c*
Hydraulic diameter (m)	0.435	0.435	0.49	0.325	0.435
2.7 ACH					
Velocity magnitude (m/s)	0.112	0.083	0.034	0.172	0.077
Turbulent intensity (%)	7.52	7.70	8.19	7.44	7.75
5.1 ACH					
Velocity magnitude (m/s)	0.214	0.159	0.065	0.328	0.146
Turbulent intensity (%)	7.15	7.32	7.78	7.07	7.36
9.6 ACH					
Velocity magnitude (m/s)	0.403	0.299	0.122	0.617	0.275
Turbulent intensity (%)	6.80	6.96	7.40	6.73	7.01

Air outlet (pressure outlet)	**2.7 ACH**
Gauge pressure (Pa)	
Backflow direction specification method	Normal to boundary
Backflow total temperature (C)	21
Hydraulic diameter (m)	0.475
Turbulent intensity (%)	
2.7 ACH	9.36
5.1 ACH	8.89
9.6 ACH	8.46

Lights (wall)	
Temperature (C)	32

Manikins (wall)	**Steady mode**
Temperature (C)	32
Mouths diameter (m)	0.016
Mouths temperature (C)	37
Inlet mouth velocity (m/s)	0
n2o mass fraction	0
	Transient mode
Inlet mouth velocity (m/s)	$1.43[sin(\frac{2\pi}{5}t) + 1]$
n2o mass fraction	0.027

5.8 CFL study

5.8.1 Transient mode and courant number

For all transient simulations, a judicious time step must be chosen and cannot be selected randomly, for the simulation to converge. The Courant number must be defined for this problem. The Courant number is a non-dimensional number to evaluate the time step requirements of a transient simulation for a given mesh size and flow velocity and is linked to the Courant–Friedrichs–Lewy (CFL) stability condition of numerical schemes.

The Courant number is defined as:

$$C = u\frac{\Delta t}{\Delta h}$$

Where u indicates the flow velocity, Δt is a representative time step of the simulation and Δh is the characteristic size of the mesh cell (in 1 dimension). For our 3D problem, the condition can be evaluated as the sum in x, y and z directions, then we have in our case the following Courant number:

$$C = \sum_i u_i\frac{\Delta t_i}{\Delta h_i} = \Delta t * (\frac{u_x}{\Delta x} + \frac{u_y}{\Delta y} + \frac{u_z}{\Delta z})$$

It indicates how much the information travels (U) across a computational grid cell (Δ h) in a unit of time (Δt). Consequently, if the Courant number is greater than one, it means that calculations are performed over several cells for one only timestep. In this case a lot of information will be lost, and the solution may either diverge or be inaccurate leading to nonphysical results. Then a high Courant number and a fine mesh does not suit because a lot of cells are not used for calculations thus it makes a detailed mesh useless. [12]
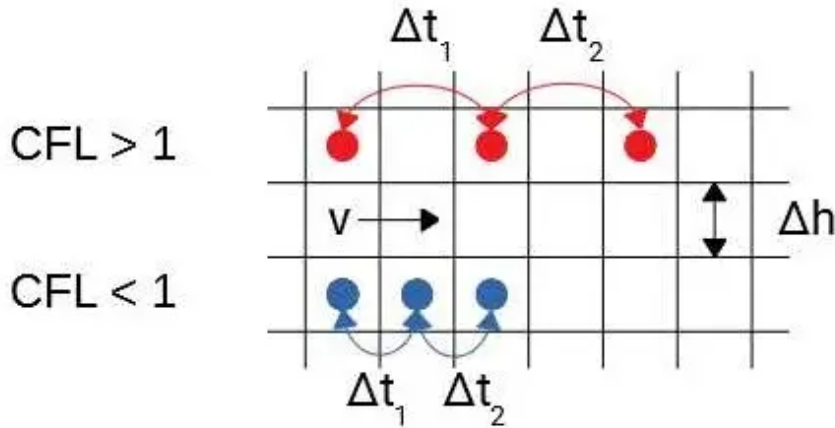
Figure 30: Representation of CFL condition and Courant number

A very fine mesh will however lead to a low Courant number and one space iteration will require numerous time iterations which will significantly increase the computational cost of the transient simulation. It is necessary to get a good compromise between space and time iteration (i.e. mesh and timestep) and this compromise had been highlighted by Courant, Friedrichs and Lewy with the CFL condition.

5.8.2 The CFL condition

The condition is expressed in terms of the Courant number as :

$$C = U \frac{\Delta t}{\Delta h} \leq C_{max}$$

Where C_{max} varies depending on the type of time integration scheme, but it is generally equal to 1 or less.

For a mesh using various mesh sizing, it is necessary to consider a part where the mesh is the finest without considering the smallest cells in these parts. Otherwise, the time step requirement will be too strict and the simulation long and costly. To avoid this, some attention should be placed on mesh quality. Small sliver cells or cells with very high skewness can create stringent time step requirements whereas only few cells are concerned by such a skewness. It is more relevant to consider the mean mesh size in a fine zone while searching for the finest cells.

In our case, the most pertinent time step is the one which take in consideration the cells near the infected manikin. Indeed, thermal gradient is high around manikins requiring a lower grid spacing. Also, the velocity is the highest due to thermal plume and breathing. The strictest CFL is obtained for the mean velocity at the mouth of the manikin that is to say 1.43 m/s which will lead to the most restrictive time step. Here we can consider that grid spacing is quite similar in every direction since face sizing function is much more dependent to other mesh functions like inflation, proximity, curvature than the direction. The mean mesh size is $\Delta h = 0.05$ m and the mean velocity is on average 1.43 m/s resulting in the following Courant number:

$$C = 1.43 \frac{\Delta t}{0.05} = 28.6 \Delta t$$

The CFL condition becomes : $28.6 \Delta t \leq 1 \Rightarrow \Delta t \leq 0.035$ s.

We can choose this value as our constant time step for transient simulation to converge. Nonetheless, in transient and pseudo-transient approaches, the time step does not need to be constant. It may even be a more efficient way to consider an adaptative time step because it avoids the two main issues of this first method considering a fixed time step:

- defining a too strict CFL condition by taking one of the worst cases as a reference in terms of local velocity and cell size (high velocity and low cell size)

- defining a CFL condition using the mean values of velocity and cell size which does not take account for refinement or face sizing.

Then we used an algorithm from ANSYS Fluent that tries to adapt the time step to the evolution of the flow (cf figure below). As an initialization for the time step, we choose the value found with the fixed timestep method, $\Delta t = 0.035$. The algorithm adjusts the time step by increasing or decreasing it in order to guarantee that the required CFL condition is met.
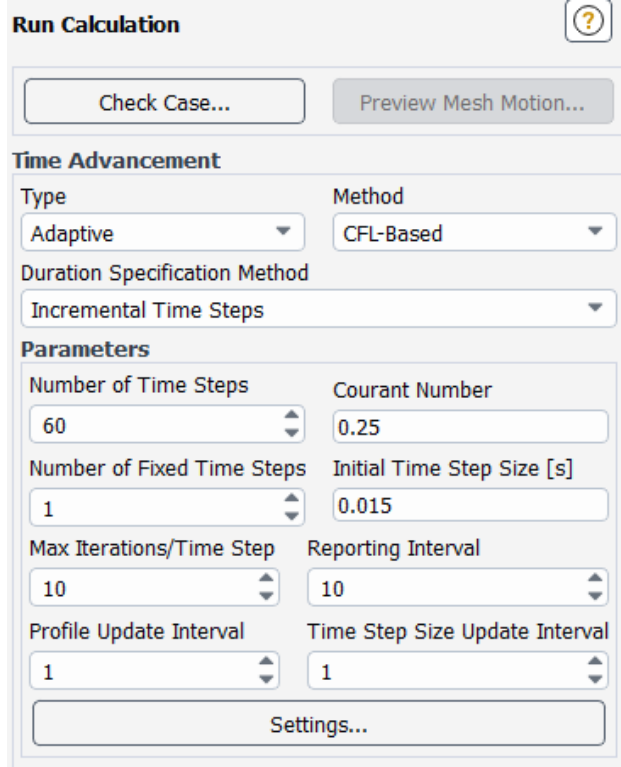
Figure 31: Adaptive timestep method

Using the adaptive method is enough precise and we observe that it was useless to use several iterations per time step since the changing time step size is always adapted to the local grid size and flow velocity. That is why implementing the simulation with 10 iterations for each time step is not valuable and then we fix it at only 1 which is sufficient for the solution to be reached with accuracy.

Nonetheless, for a CFL of 1 the adaptive method use a low time step with an order of magnitude of 10^-5, which is not adapted to a simulation over several minutes. To compare with the experimental results, the simulation has to last 20 minutes on average which represents 24 million iterations. This is not realistic and feasible in this thesis. We then need to use a fixed method and to find a reasonable time step for the solution to converge.

To solve this issue, we consider the CFL condition in the locations where the mesh is the coarsest to determine a range of values for the time step. We sum up the different values in the following table to make the reasoning more understandable.

	Fine region (mouth of the infected manikin)	Coarse region (spacing without mesh adaptation in low gradient zones)
Mean velocity $[m/s]$	1.43	0.05
Averaged grid spacing $[mm]$	0.05	0.1
Time step for CFL condition $[s]$	0.035	1.54

Table 1: Range of valid time steps

Finally, we have to find a time step giving a good convergence, at least the same order of magnitude for the residuals obtained with the steady state simulation and respecting the next condition:

$$0.035 < \Delta t < 1.54$$

We could also find an optimal courant number higher than 1, using the adaptive method and still converging with the same residuals and then reading the time step used by fluent. Nevertheless, the real calculation for the courant number in this simulation is much more complex, and it becomes harder to get a good control over the simulation and what happens in the software.

Then, we compare the residuals for different converged simulations using various time steps with the corresponding number of iterations needed to reach a 20-minute simulation of the manikin's breathing. It is the time found in the experimental thesis to reach the steady state for tracer gas concentration. We also need to adapt the controls parameters over the simulations.

From a timestep of 0.1s and higher values, some variables start to diverge thus the associated control must be corrected. For example, turbulent dissipation rate factor, epsilon, is not fully converged and the residuals are oscillating between 10 and 10^{-2}. We can have several strategies to solve this problem and get a better solution for one fixed time step:

They are set by default by the ANSYS Fluent but it is possible to make the calculations for one parameter more accurate.

- identify if some parameters are diverging as above and change the control values linked to these parameters.

- increasing the maximum number of iterations per time step.

  Indeed, the software indicates the number of iterations for each time step. The user just fixes the maximum value, commonly 20, and the residuals he wants for every parameter then Fluent adapts this number at each time iteration. If the residuals, for one space iteration, are reached after only 4-time iterations, it jumps to the next cell and calculate again the time iteration.

- increasing the maximum number of iterations per time step :
  - - modify significantly the range of valid time steps for our simulation
  - - start again with a mesh which is too fine so restrictive regarding the CFL condition

The comparative study for time step is shown below. For each simulation, time step, iterations required for 20 min of breathing (with one max iteration per time step so need to multiply by the avg iterations per time step) and order of magnitude for residuals (i for an order of magnitude of 10^{-i}) are presented:

Time step	Iterations per time step	Turb model	Total iterations required	Continuity	Velocity	k	epsilon	Energy	N2O
0.01	7	RNG-standard	840 000	3	4	4	2	7	4
0.05	20	RNG-standard	480 000	3	3-4	3-4	2	7	3-4
0.1	40	RNG-standard	480 000	2-3	4-5	3-4	2	6-8	2-3

Figure 32: Time step study

These results are obtained with the unstructured mesh and with average iterations per time step, got thanks to data sampling. The upper limit has been put at 40 iterations to limit the time of one entire simulation which is already too high. Indeed, the average time to compute one iteration is about 3.5s then the whole time required for the shortest simulations with unstructured mesh is 467 h i.e. 19.4 days. This shows the unstructured mesh is unusable in a transient simulation as our case. Furthermore, simulations with time steps higher than 0.1 s lead to diverging results that is why no additional data has been collected.

A similar approach has been realized with the structured mesh. The best compromise between time step and iterations per time step with fixed convergence as reference as led to the following values:

Time step	Iterations per time step	Turb model	Total iterations required	Continuity	Velocity	k	epsilon	Energy	N2O
0.075	7	RNG-scalable	112 000	4	4-5	4-5	2-3	6-8	3-4

Figure 33: Final time step case for structured mesh

As expected, the structured mesh is more accurate and with 0.075 as time step, we need only 5 iterations to reach convergence with lower residuals. Averaged duration of one time step, including 7 iterations, is 25s. Therefore, the final time required for realizing one simulation is 111h which represents 4,6 days of simulation. At this point, two strategies are conceivable:

- to make the mesh coarser again

- to use more powerful computers for calculations

If the first option appears as an easier solution, it is difficult to make the mesh coarser since it has already less than 1 million of cells for a 6-m room then it would give inaccurate results. Furthermore, we could only increase global sizing since every face sizing are realized to get a good mesh quality and avoid unacceptable values of quality mesh parameters.

6   Results

6.1   Validation model

As stated in this thesis, it is important to validate the model we built. To ensure our model is valid and loyal to real airflow behaviour and tracer gas diffusion in the room, we compare data collected from simulations to experimental data obtained in the parallel study. To proceed the same way, we measure n2o concentration at mouth of the exposed manikin M_{exp}, at its left and right shoulders (20 cm left and right respectively from the mouth center and 5 cm below the breathing zone) and at exhausts. This data was realized at 5.1 ACH and 1-meter distance between manikins.

We choose here to show the nearest and the furthest locations to be more efficient, namely mouth and exhaust. The curves for shoulders can be found in appendix.

Graphs shows 3 different curves : experimental data (-exp) and theoretical data with and without DO radiation model.
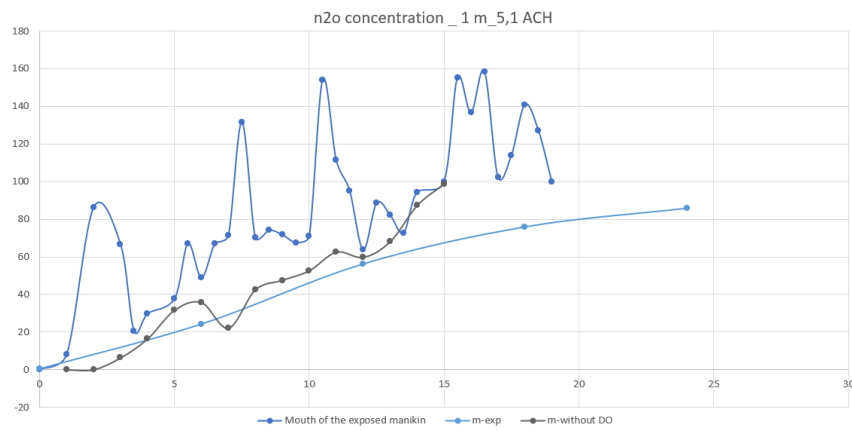
Figure 34: Validation model at mouth location
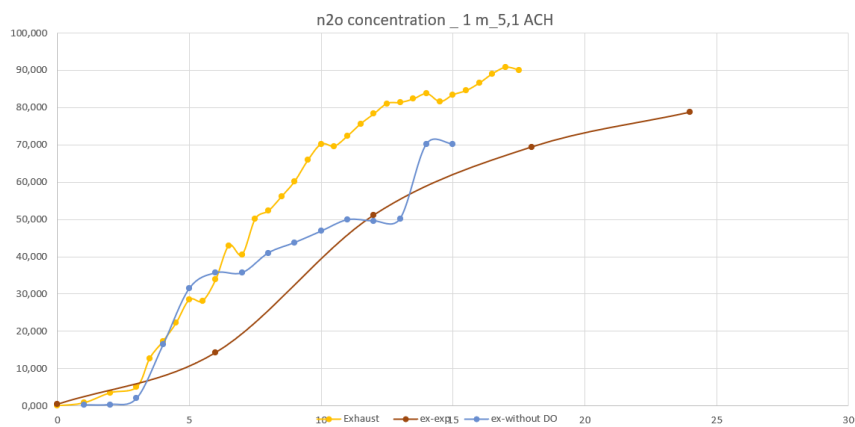
Figure 35: Validation model at exhaust location

The results are presented in ppm (volume) to be compared to experimental data whereas data is collected from simulations as tracer gas mass fraction.

$$ppm = w * \frac{\rho_{tot}}{\rho_{air}} * 1000000$$

where w is n2o mass fraction and $\rho_{tot}=\rho_{air}+\rho_{n2o}$.

It can be written as :

$$ppm = w * [\frac{\rho_{n2o}}{\rho_{air}} + \frac{\rho_{air}}{\rho_{air}}] * 1000000$$

$$ppm = w * 2.53 * 1000000$$

as relative density of n2o is 1.53.

We may also note that steady state is reached around 25 minutes.

Moreover, at we rapidly observe that simulation data was better without radiation model (explained in Discussion part), we realize other simulations without such a model.

6.2 Different ACH

In this section, we will focus on 1-meter distance between the two manikins.
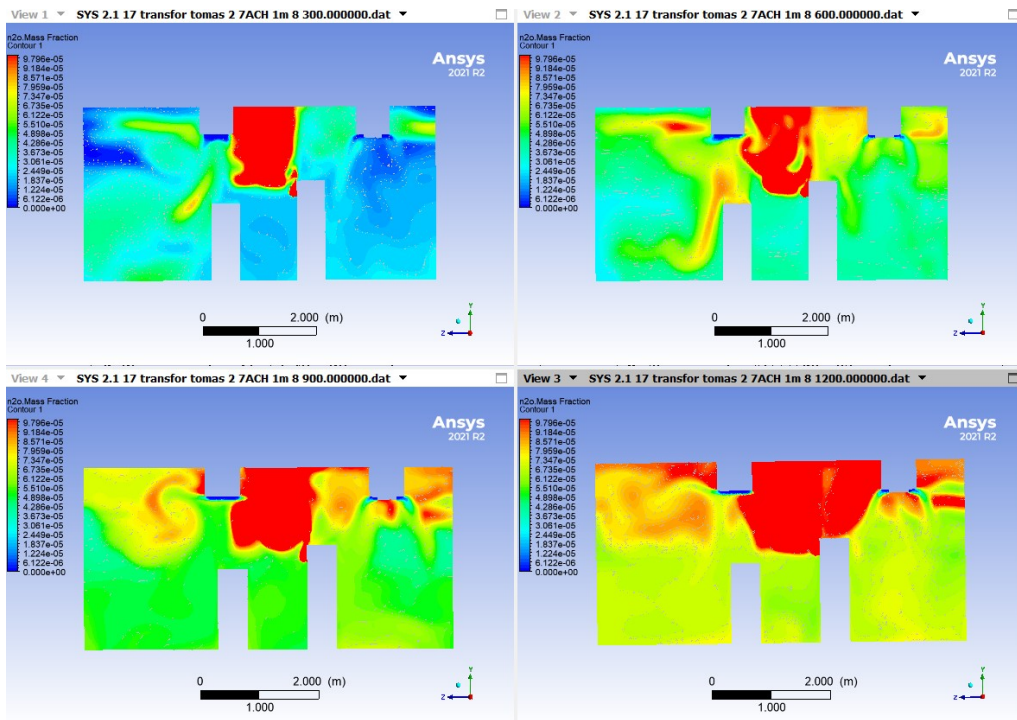
Figure 36: n2o - 2,7 - 1m
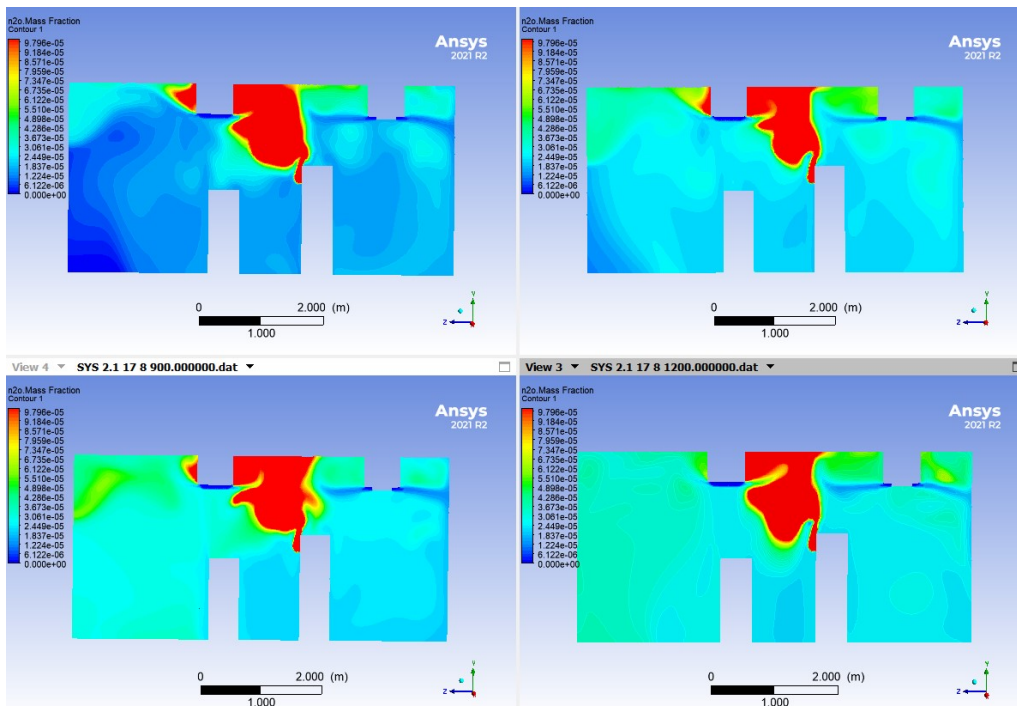
Figure 37: 9.6 ACH
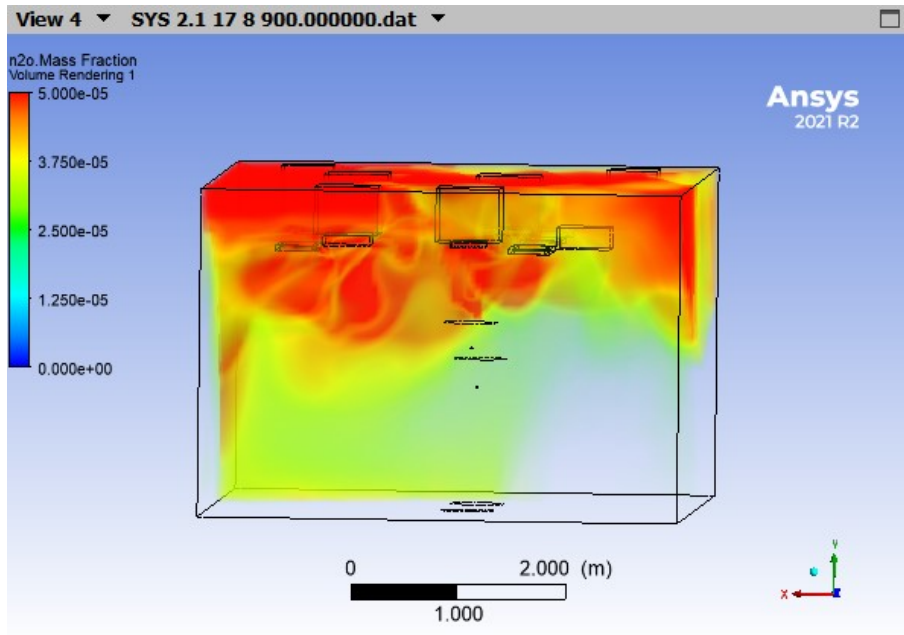
Figure 38: 9.6 ACH, n2o volume rendering

Temperature in a vertical plane located at the center of the room and volume rendering are shown at 2.7 ACH but we note same temperature behaviour in every ACH cases.
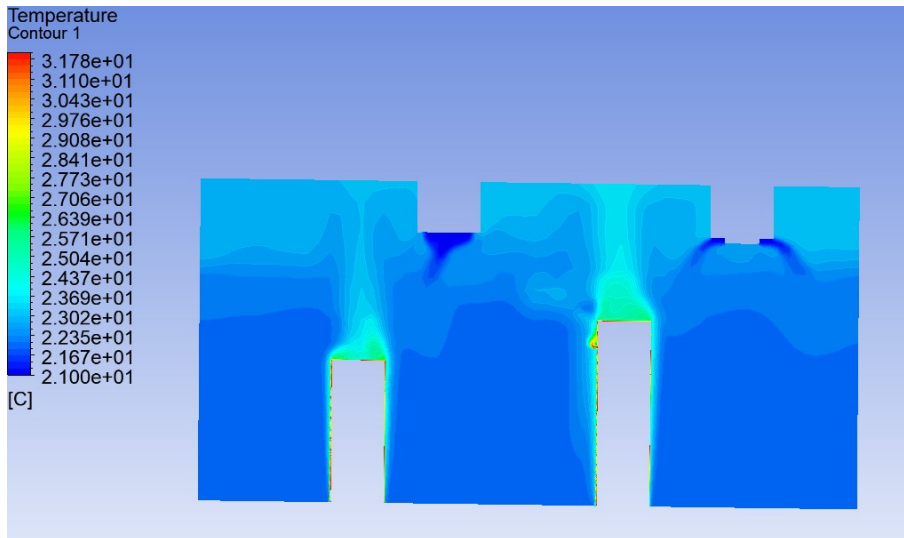
Figure 39: Thermal plume
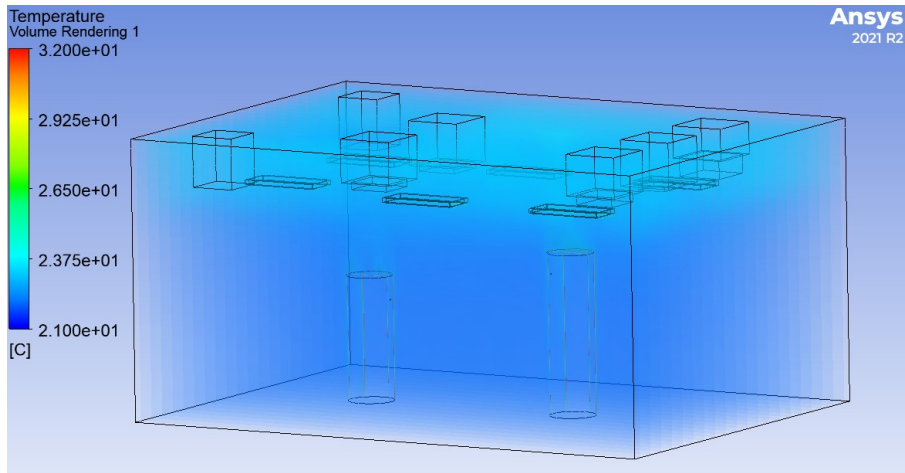
Figure 40: Temperature stagnation level

6.3 Distance comparison

We will consider here the 2.7 ACH case with a 2-meter distance separating manikins. We use the same scale as before to compare the results.
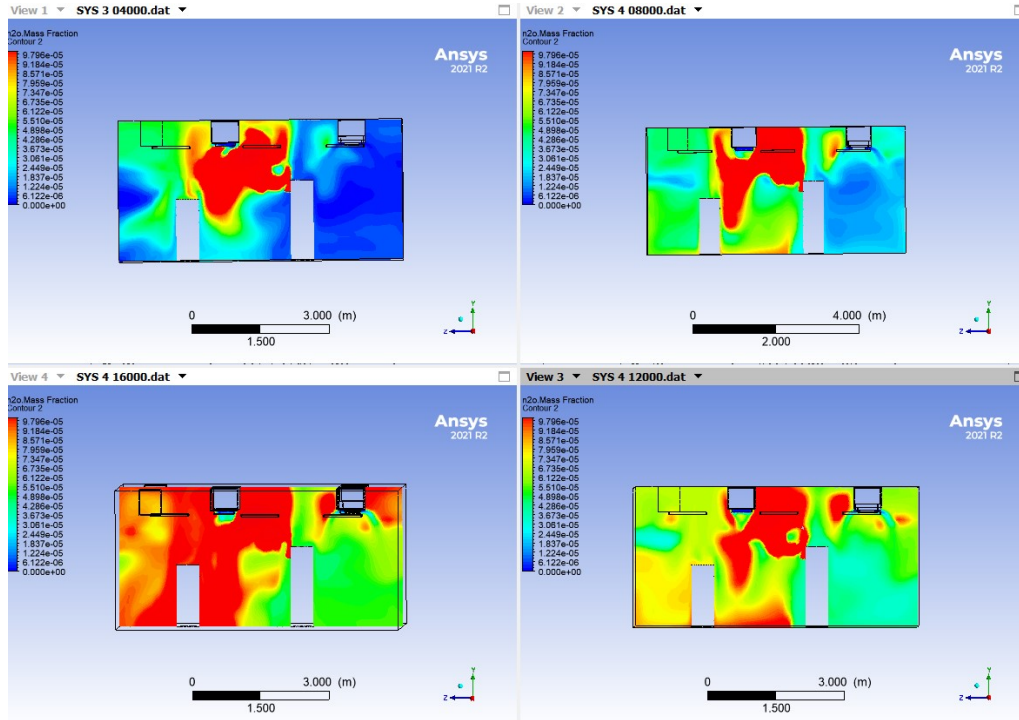
Figure 41: n2o mass fraction - 2.7 ACH - 5, 10, 15 and 20 min

Then, we adapt the scale to see in a better way the phenomenon of n2o diffusion in the room. We consider here the final steady state (based on n2o concentration in the room) of transient simulation. We consider same scale for 1-meter and 2-meter case.
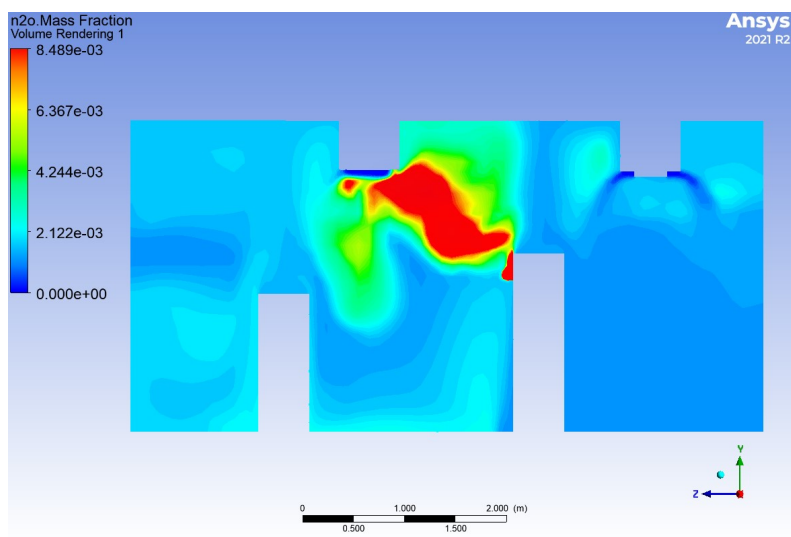
Figure 42: n2o mass fraction - 2.7 ACH - 2m - 30 min
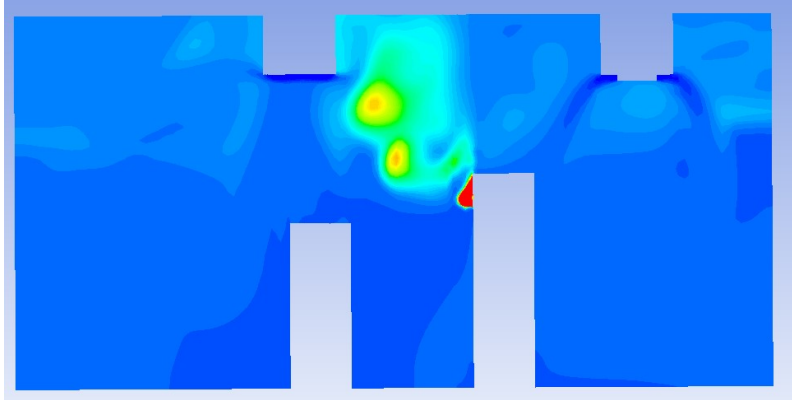
Figure 43: n2o mass fraction - 2.7 ACH - 1m - 30 min

7 Discussion

7.1 Radiation model

In some literature reviews regarding radiation model in indoor ventilation (REF) it can be found that this model can be used and give accurate results. With the previous difference temperature of our case of study, it could be then valuable to use the Discrete Ordinates model. However, if the model worked well for the first cases (1m- 2,7ACH and 5,1 ach), it started to diverge for every other cases. We then searched from where could come this problem and after deactivating the radiation model the solution was converged with lower residuals. Moreover, the solution was calculated in a faster way. We tried to understand how the radiation model could have led to such divergence and why it was working for the 1m case.

We didn't't have enough time to prove the reason why, but it is probably the fact that when the manikins are really close to each other there is an entire zone, between them, where the temperature is higher than in the other parts of the room. In this zone, the flow has more difficulties to go and then the heat is stuck and absorbed by the surface body of the manikins. Therefore, there is a significant part in the room where there is a higher temperature while in the other case the two manikins are far thus they have a little influence on each other leading to really low temperature variations in the room which could explain that the radiation model is not correct in the 2 m case. Furthermore, another temperature argument points out the radiation model cannot be valid in this case. Indeed, averaged room temperature are

Another explanation could be that the radiation model need temperature boundary conditions since it works with temperature differences in the room. In this model, we do not use temperature BC at the walls, they can absorb heat without temperature restrictions . So manikin surfaces which are the main temperature BC may absorbs too much heat because this is the main place where the radiation model will affect our case. This excess of heat absorption could explain the excess of 1.5 degree Celsius in the case with radiation model compared to the case without such a model (23.8 for 5,1 ACH 1 m with DO and 22.3 for 5,1 ACH-2m without). There is still obviously a temperature difference between the 1m and the 2m cases, however 1.5-degree difference is too high and cannot be explained only by the distances between the manikins. That is why it was required to wonder how the radiation model is interacting with the room.

7.2 Buoyancy

Thermal plume

as said in the method part in geometry in manikin, thermal plume is continuous and uniform at surface body

Temperature stagnation

We may observe temperature layers at specific stagnation temperature. This is the consequence of neglecting vertical velocity. The most significant development of the airflow appears as horizontal diffusion which creates these layers and explain why contaminant is stuck above manikins. As vertical velocity is also lower than horizontal one in real case, we may assume that a stagnating airflow in the room at this height (2.5 to 3 m). This phenomenon is also due to the type of HVAC system in the laboratory room. Every inlets are located on the ceiling, and combined with main velocity displacing in a horizontal plane, it leads to such a stagnation phenomenon.

This stagnation level is stratified as we can see in figure 39 but becomes really consistent at about 2.5 m height.

7.3 Tracer gas

Validation model considerations

Theoretical n2o concentration is higher at exhaust in the beginning of the simulations then it becomes similar to experimental data. It seems diffusion of airflow in our model is faster than in real conditions. It may be explained by the tracer gas modelling in ANSYS which results in higher diffusion coefficient J_i then n2o gas reaches earlier exhausts but stabilize at same concentration value.

Also, the theoretical curves at mouth location shows higher n2o concentration than same concentration obtained experimentally. We may assume that measurements at the mouth of the exposed manikin was not realized directly at the mouth but there was a distance between the measurement device position and the effective location of the mouth for practical reasons. However, in simulations we measure contaminant concentration at the exact location of the mouth center. Then, it is strongly possible that some of contaminant particles were deposited on the surface of the mouth representing an additional concentration. This can explained why theoretical data at the mouth is higher than experimental data whereas it is the opposite way for left and right shoulder (i.e. Appendix).

We can note in validation model graphs (Results → Validation model) that the CFD model give some additional information on n2o concentration at specific locations used in the experimental study. Instead of having a smooth curve, we may observe there are peaks of risk infection every 5 seconds, which means there is more risk of contamination during exhalation than the mean risk shown in experimental data, obtained every 6 minutes.

Different risk for different distances

In the case of different distances between manikins, we observe a higher tracer gas concentration in the 2-meter case than in the 1-meter case. In every cases, tracer gas goes up due to diffusion and thermal plume of the sitting manikin. Moreover, at this height there is a temperature stagnation (see Buoyancy discussion part), which lead to a stagnating cloud of contaminant between the manikins. Nonetheless, Figure 42 shows an additional feature. A part of this cloud is not stuck at this location but is re-entrained in the breathing zone (due to inlets in the middle of the room) of the exposed manikin which may explain higher concentration in experimental data (comparative study) when manikins are further from each other. Indeed, if this phenomenon exists in the 1-meter case (at lower concentration values), the cloud will go further than the manikin and will not have any consequences over the contamination risk of the exposed manikin.

Furthermore, one appalling observation we can make thanks to figure 42 and figure 43 is that averaged n2o mass fraction in the room has more important value in the first case. We think that

in the 2-meter case, as the flow is re-entrained in the breathing zone, it may be stopped by thermal plume of the manikin, reducing velocity of the flow in the upper region above the manikin on the right side. Then, there is struggle between inlets which deflects the flow in lower zones and thermal plume in higher zones. That is why we can see an air curtain on the right side of M_{exp} creating a stagnating contaminant cloud at this location. The air curtain prevents the flow from displacing above M_{exp} and a fewer part of the flow can be evacuated through the outlets leading to a higher mean tracer gas concentration in the room.

8 Conclusion

This project was overall very interesting and educational. A lot was learned about indoor environment, airborne transmission and CFD techniques. The comparative study has allowed our thesis model to be validated with experimental data to create a loyal model of what happens in the real laboratory room.

Furthermore, we found similar results regarding n2o concentration at relevant specific locations such as the mouth of the exposed manikin. We also observed a crucial phenomenon being a higher contaminant concentration when the manikin are two meters away than distanced by only 1 meter.

As the experimental study could not proved what was the origin of this phenomenon due to limited measurement points, CFD study shows that the specific configuration of the room combined with the 2-meter case makes thermal plume and entering airflow from centered air supplies act in a way that the flow cannot reach the outlets as it was in the 1-meter case. An air curtain is created and both thermal plume and inlet velocity prevent the flow to displace to the other side of the room and accentuates the contaminant stagnation zone. Indeed, air curtain added to existing stagnation temperature lead to a larger zone where there is a high Covid-19 particle concentration. This zone even extends over the breathing zone of the exposed manikin. Consequently, there is an important risk of contamination when the manikins are far from each other. However, this case is specific to this geometry room, this HVAC system, the 2-meter distance and cannot be expanded to other studies. It is, though, interesting to note that in some particular cases, our common sense can be thwarted and the 1-meter security distance is not applicable and may even be counterproductive.

Nevertheless, improvements could be done on our CFD model. In particular, if thermal plays a such significant role in the air curtain creation, it may be relevant to use CTM in order to obtain manikin thermal plume distribution with high accuracy. A well defined thermal plume would allow determining how the breathing zone of the manikin is influenced by the air curtain and how much airflow rate is perturbed.

9   References

[1] Hadi Borbar and al.,2021, A simplified model to estimate COVID19 transport in enclosed spaces, research gate

[2] Jianchia Ma and al., 2021, What dominated personate exposure? Ambient airflow pattern or local human thermal plume, Building and environment 196

[3] Sun et al., 2020, How human thermal plume influences near-human transport of respiratory droplets and airborne particles: a review

[4] Chudecka and Lubkowska, 2015, Thermal imaging of body surface temperature distribution in women with anorexia nervosa, research article

[5] Nielsen and al., 2007, Computational Fluid Dynamics in Ventilation Design, REHVA

[6] Gao and Niu, 2005, Transient CFD simulation of the respiration process and inter-person exposure assessment, Building and Environment 41

[7] Menchaca-Brandan, Dominguez Espinosa, and Glicksman, 2016, The influence of radiation heat transfer on the prediction of air flows in rooms under natural ventilation. Energy and buildings 138

[8] Russo - Basse., 2016, Scaling of turbulence intensity for low-speed flow in smooth pipes. Flow Measurement and Instrumentation 52

[9] Lui et al., 2019, A Review of CFD Analysis Methods for Personalized Ventilation (PV) in Indoor Built Environments, Sustainability

[10] ANSYS, Inc, 2013, ANSYS Meshing User's Guide

[11] https://www.idealsimulations.com/resources/courant-number-cfd/

[12] Rencken et. al, 2021, 'Patterns of sars-cov-2 aerosol spread in typical classrooms', Building and environment 204

[13] Johns Hopkins Medicine (-), 'Vital signs (body temperature, pulse rate, respiration rate, blood pressure)

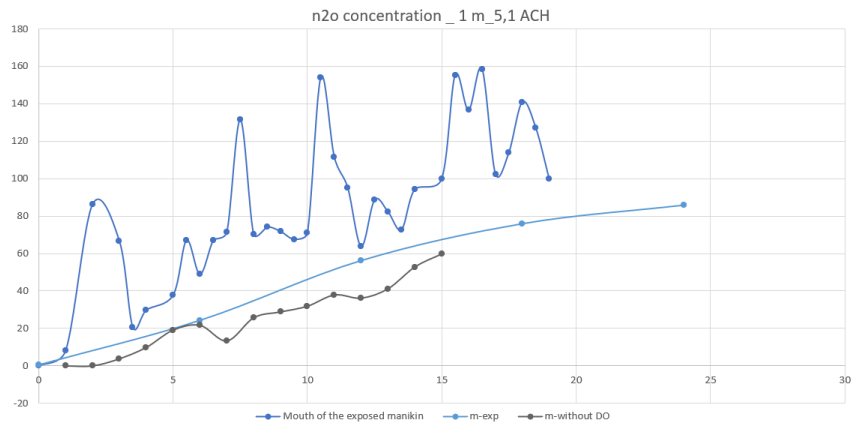# 10 Appendix

10.1 Validation model graphics

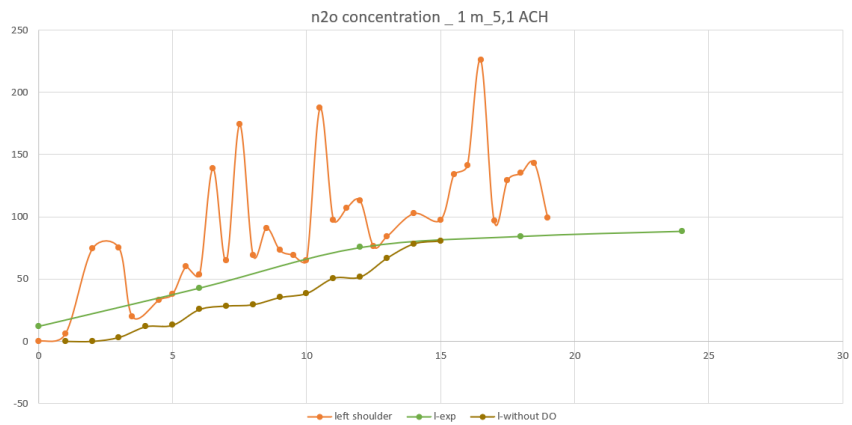Figure 44: Validation model at mouth location

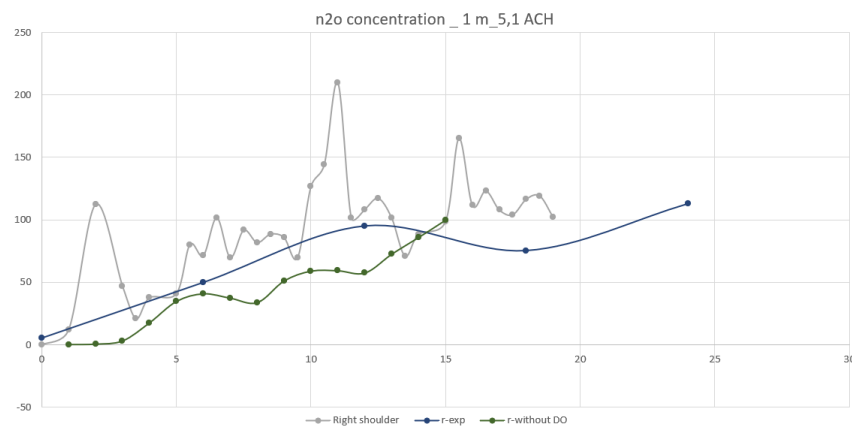Figure 45: Validation model at left shoulder location
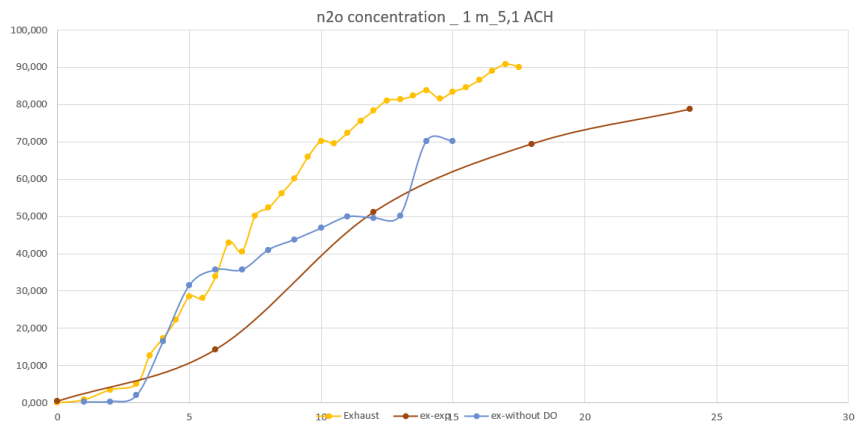

Figure 46: Validation model at right shoulder location

Figure 47: Validation model at exhaust location

10.2 Relevant experiment data

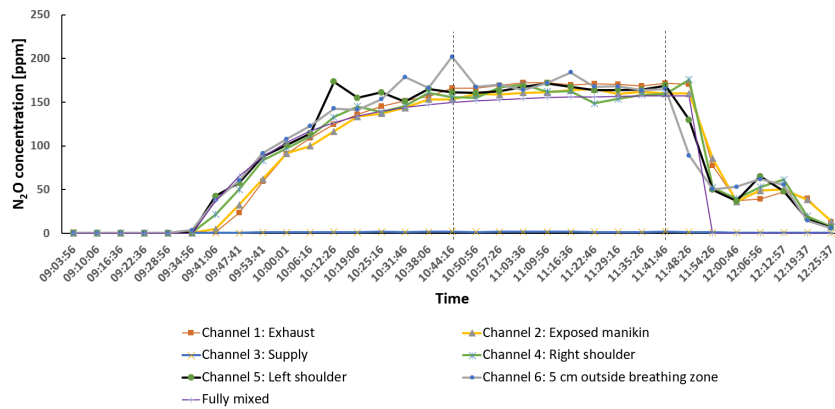Experimental data from the comparative study, useful in this thesis, is presented below :

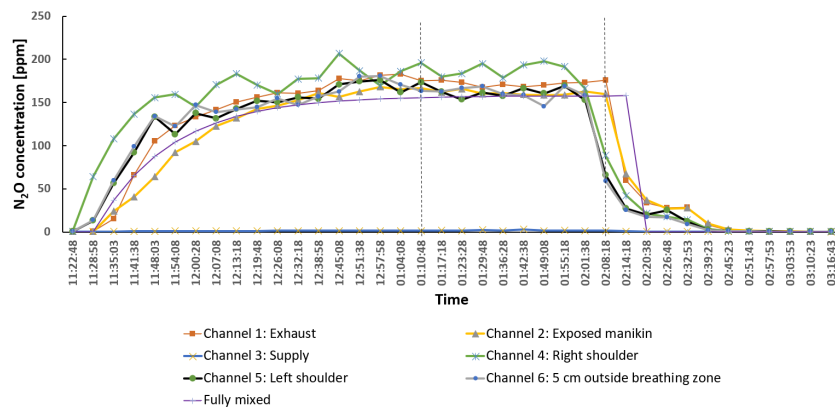Figure 48: 2.7 ACH -1m - experimental data
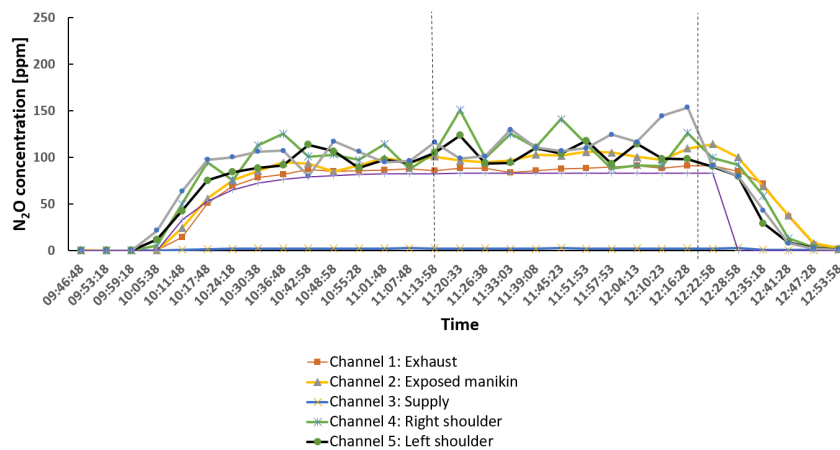

Figure 49: 2.7 ACH -2m - experimental data
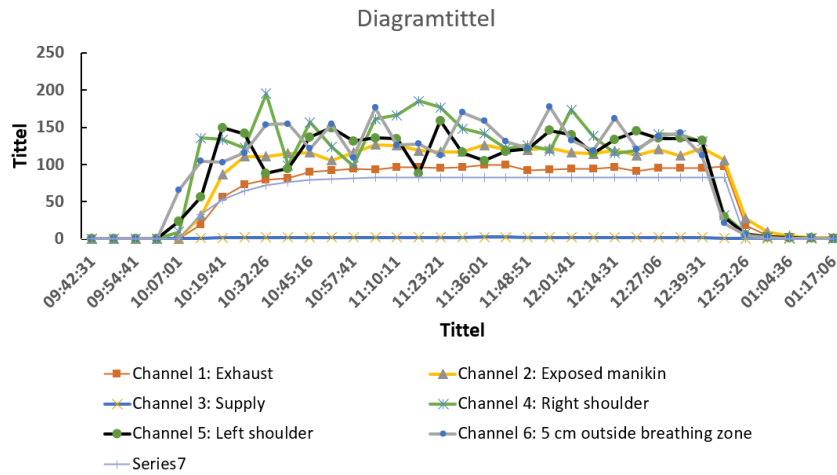

Figure 50: 5.1 ACH - 1m - experimental data

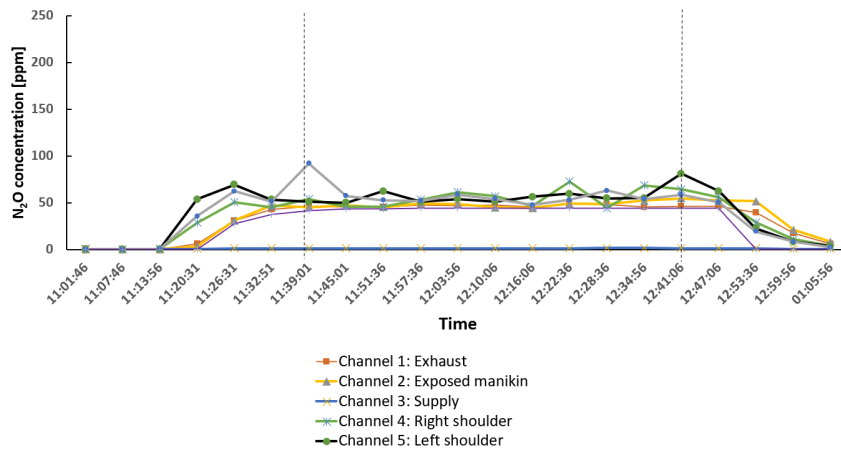Figure 51: 5.1 ACH - 2m - experimental data
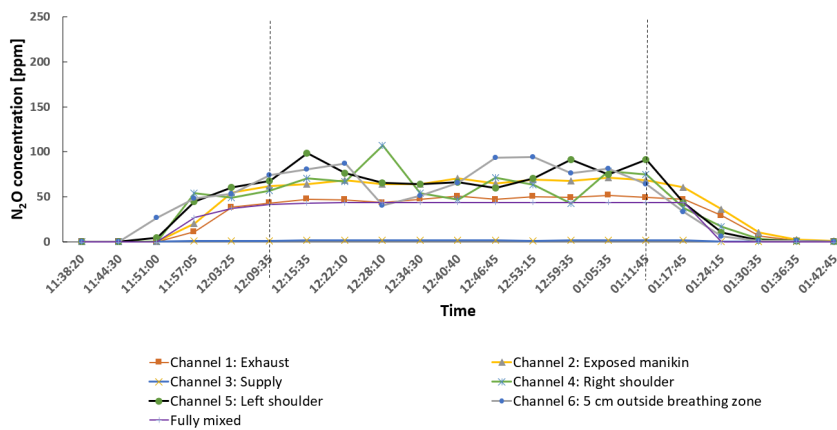

Figure 52: 9.6 ACH - 1m - experimental data

Figure 53: 9.6 ACH - 2m - experimental data